Title

X-RAY PHOTOEMISSION STUDY OF THE ELECTRONIC STRUCTURE OF THE 3d TRANSITION METALS Sc TO Zn

Authors

Ley, L.
Kowalczyk, S.P.
McFeely, F.R.
et al.

Publication Date

1974-05-01

Submitted to Physical Review B

LBL-2929
Preprint

X-RAY PHOTOEMISSION STUDY OF THE ELECTRONIC STRUCTURE OF THE 3d TRANSITION METALS Sc TO Zn

L. Ley, S. P. Kowalczyk, F. R. McFeely, and D. A. Shirley

May, 1974

Prepared for the U. S. Atomic Energy Commission
under Contract W-7405-ENG-48

DISCLAIMER

X-RAY PHOTOEMISSION STUDY OF THE ELECTRONIC STRUCTURE OF THE 3d TRANSITION METALS Sc TO Zn*

L. Ley†, S. P. Kowalczyk, F. R. McFeely, and D. A. Shirley

Department of Chemistry and
Lawrence Berkeley Laboratory
University of California
Berkeley, California 94720

May 1974

ABSTRACT

High-resolution XPS spectra of the 3d metals have been taken under ultra-high vacuum conditions. Several major features of the valence bands have been observed for the first time. In hcp Sc and Ti, two main peaks were identified and compared with theoretical band structure results: some rigidity in the bands is apparent here and in bcc V and Cr, in which the expected two-peak structure was resolved. In Cr, a very low density of states near the Fermi energy E_F was observed for the first time by high-energy methods. Neither UPS nor SXS has shown this before. A detailed comparison of the Cr spectrum with theory was made, and symmetry-point energies were assigned. The valence band spectrum of Fe was interpreted in detail, showing excellent agreement with expectations based on a band model of ferromagnetism. Of special importance is the observation of a relatively low density of states at E_F, with a peak just below E_F. The valence bands of bcc iron could be constructed from two sets of bcc Cr bands, shifted to account for spin polarization. Symmetry-point energies for Fe were deduced for the first time. The Co and Ni spectra showed detailed agreement with theory. In Cu, symmetry-point energy differences were

derived and compared critically with predictions of eleven theoretical calculations. The general agreement of these results with theory is encouraging, although many ambiguities remain. This work may provide a basis for discussing the valence bands of the 3d metals as a complete group. Structure was observed in the 3s peaks of several metals. The light metals Sc, Ti, and V showed asymmetric 3s lines attributable to many-body effects. The (paramagnetic) antiferromagnets Cr and Mn showed 3s multiplet structure attributable to localized moments. Similar structure in ferromagnetic Fe, Co, and Ni was less distinct. In Cu and Zn, with filled 3d shells, the 3s lines exhibited no multiplet splitting.

I. INTRODUCTION

The 3d transition elements comprise an interesting group of metals, exhibiting a wide variety of structural and electromagnetic properties. A key factor in the understanding of these metals is the peculiar nature of their electronic band structures. The valence bands may be considered to arise from two nearly degenerate atomic levels, the 3d and 4s. These levels, however, have very different spatial distributions, with the 4s electrons extending considerably beyond the average radius of the 3d shell. Thus the valence bands are of two distinct types, a wide band of predominately 4s character resembling the valence bands of simple metals, and a set of narrow, more correlated d-like bands. The s-like electrons are believed to be the primary source of bonding in the metals,[1] while the narrow atomic-like d bands give rise to such phenomena as ferromagnetism.[2]

Because many theories of the magnetic properties of the transition metals take d-bandwidth, total bandwidth and density of states at the Fermi level as essential one-electron properties responsible for the magnetic behavior, it is clear that a detailed and quantitative knowledge of the valence-band density of states $N(E)$ is essential. Electronic specific heat data, conductivity measurements, and the de Haas-van Alphen effect, to mention only a few, sample the electronic properties only within $\sim kT$ of the Fermi energy; thus information on the more tightly bound states is necessarily indirect. Spectroscopic methods such as soft x-ray emission spectroscopy (SXS),[3-6] ultraviolet and x-ray photoemission (UPS, XPS)[7-16] and optical reflectivity measurements are free of these limitations and have contributed valuable information about the overall features of $N(E)$ for most of the materials under consideration here.

A straightforward interpretation of SXS and low-energy ($h\nu \lesssim 40$ eV) UPS data in terms of only the initial density of states is not possible in most cases. In SXS, the initial-state core vacancy may distort the valence-band density of states severely. Examples of such distortions are well documented in the emission spectra of the alkali metals.[17] Low-energy UV photoemission spectra are commonly interpreted in one of two ways; the direct transition model,[18] in which $\vec{k}$-conservation is an important selection rule and the non-direct-transition model.[19] In either case the measured spectrum will contain features reflecting both the initial electron state and the final electron state subject to the restriction of energy conservation. Starting with a reliable band-structure calculation, an interpretation of the UPS spectrum in terms of initial- and final-state properties is possible, and it can yield very detailed results.[20] The method is, however, very involved, and it has so far been applied in a rigorous way to only a few cases.

With increasing excitation energy $h\nu$, the $\vec{k}$ selection rule is readily fulfilled without introducing additional structure. This is expected from the high and uniform density of available states over the whole range of $\vec{k}$-space at energies large compared to the energy variations of the lattice potential. Experimental evidence for this fact is well documented,[21] and an interpretation of high energy ($h\nu \gtrsim 100$ eV) spectra in terms of initial state density has been highly sucessful.[22] It is our objective in this paper to present a systematic XPS study of the density of states of the first row transition metals from Sc to Zn. Experimental details are given in Sec. II and results are presented in Sec. III. Some of these elements (Fe, Co, Ni, Cu) have been studied earlier by XPS,[14-16] but the improvements in resolution and vacuum conditions obtained in the present study yield new results even for these cases, as discussed in Sec. IV.

In addition to the valence-band spectra, XPS offers a unique spectroscopic method for the investigation of unpaired spin density on an atomic site, via the multiplet splitting of core-electron binding energies.[23,24] In the 3d series, the splitting of the 3s level gives a sensitive measure of the product of exchange coupling strength and unpaired 3d spin density. In the 3d transition series, there are "normal" paramagnetic metals Sc, Ti, V, Cu and Zn, antiferromagnets Mn and Cr, and ferromagnets Fe, Co, and Ni. The 3s spectra of all of these elements have been measured and are discussed in relation to their magnetic properties in Sec. V.

II. EXPERIMENTAL

All the specimens were studied in a Hewlett Packard 5950A electron spectrometer with a monochromatized Al K_α (1486.6 eV) x-ray source. The instrumental resolution is 0.55(2) eV as previously measured from the broadening of the sharp Fermi edge of a number of metals.[25]

The spectrometer has been modified for ultra-high vacuum operation, and was baked out at 200°C before the start of this series of experiments, obtaining a base pressure of $< 2 \times 10^{-10}$ Torr. All the samples were prepared in situ. Films of Ti, V, Cr, Mn, Co, Ni, and Fe were prepared by d. c. sputtering from high purity single crystals onto stainless steel substrates in an ultra pure argon atmosphere. Sc, Ti, V, Ni, and Cu specimens were prepared by vapor deposition onto stainless steel substrates. Ta or W filaments were used and the evaporation charges were either single crystals or ultra pure (better than 99.99%) polycrystalline material. Before evaporation, the filament and charge were vigorously outgassed. In most cases, the vacuum during evaporation was 1×10^{-9} Torr or better, and the worst case was 5×10^{-9} Torr. Samples of Co, Ni, Cu, and Zn were also prepared by argon ion bombardment of single crystal disks, which had been mechanically polished and electropolished before insertion into the vacuum system. The different methods of sample preparation gave identical valence-band spectra in all cases except Cu. The Cu result presented in Sec. III is that of a single crystal, which showed the best resolved fine structure. Each sample was thoroughly checked for impurities such as imbedded argon, surface contaminants (oxygen and carbon), and possible evaporated filament material (W, Ta) immediately after preparation, by scanning the region from 0 - 1280 eV binding energy. In addition to the wide scans, 20 eV scans of the O 1s and C 1s regions were monitored. The only contamination observed in these

experiments was oxygen. The spectra reported here are from specimens on which no oxygen signal could be observed initially. Some of the metals showed oxygen build-up in the course of the measurements; however, no photoemission lines were ever detected which would conform to the formation of an oxide, even from samples with the largest oxygen 1s signals. Whenever the oxygen signal reached a level of $\sim$ 0.5 monolayer coverage of O_2, a new sample was prepared.[26] Only the Cr VB spectra had an accumulation time ($\sim$ 6 hrs) which resulted in a final oxygen coverage of 1.2 monolayers. In this case, short runs on freshly prepared, clean samples gave undistorted valence band spectra. On the other hand, a scandium specimen could be kept in the spectrometer vacuum for over 24 hours without any detectable oxygen buildup. The typical time for the measurement of a valence band spectrum was about 8 hours.

III. RESULTS

The XPS spectra I(E) of the valence electron region of the transition metals scandium through zinc are shown in Figs. 1-3. These spectra have had smooth background contributions from inelastically scattered electrons subtracted under the assumption that each point in I(E) contributes to the inelastic tail in proportion to its initial intensity. The solid curves are meant only to guide the eye and indicate the real structure in I(E).

Structural features (i.e., characteristic peaks, shoulders and edges) of the XPS valence band spectra I(E) of each element are denoted by letters in Figs. 1-3 and the energies (referred to the Fermi level E_F) are given in Table I. Sharp decreases of intensity at E_F in Sc, V, Co, and Ni define E_F to $\pm$ 0.05 eV. This standard allows us to fix the position the Fermi level in the remaining spectra. At the other end of the valence bands -- the "bottom" or high binding energy limit -- it is more difficult to establish exactly where the bands end, although XPS spectra tend to be more readily interpretable in this respect than either SXS or UPS data. Most of our spectra show some tailing at the "bottom" of the valence bands. This tailing may be a real physical effect or it may result from imperfect correction for scattering. In any case some interpretation is necessary to assign the positions of the bottoms of the valence bands. In zinc, the low energy limit of the 3d bands, and presumably of the valence bands, is defined by the sharp decrease in the d-band peak intensity. The bottom of the valence bands is well defined for Sc, Fe, and Ni by the negative curvature of I(E) in this region. The spectra of Ti through Mn exhibit a slight kink as I(E) joins the essentially flat background. In Co and Cu, the determination of the bottom of the valence band is more difficult because in this region I(E) connects smoothly with the background. We will return to this problem, when we discuss the spectra in more detail in Sec. IV.

IV. DISCUSSION

A. Comparison with Other Experimental Results

As mentioned earlier (Sec. I), the interpretation of low energy UPS, SXS, and XPS spectra in strictly comparable terms is not possible. That being true, a direct comparison of the original experimental spectra should be equally limited. This is clearly indicated, when we compare, as an example, the valence band spectra of Cr obtained by the three different methods (Fig. 4). The soft x-ray spectrum (SXS) is taken from Fischer;[4] it represents the Cr(2p-hole) → Cr(VB-hole) transition. The UPS spectrum is from Ref. 12 and the XPS spectrum is from this work. We see immediately that the three spectra hardly resemble each other except for having a region of high electron intensity around -2.0 eV with similar widths, of 4.9 eV (XPS), 4.6 eV (UPS), and 4.5 eV (SXS) measured as the full width at half maximum (FWHM). The energies of the fine structure vary considerably from spectrum to spectrum in Fig. 4.

The reasons for these discrepancies have been mentioned before. They are methodical rather than experimental in nature. The recently measured SXS spectrum of Ti[6] similarly shows disagreement with the XPS data, whereas UPS and XPS spectra exhibit quite detailed agreement in this case.

The conclusion to be drawn is that a direct comparison of low-energy UV and our XPS spectra is in principle meaningless. The degree of actual correspondence can however be interpreted as a measure of the structure introduced into the UV spectrum by the final states, together with differences in cross-section modulation between XPS and UPS.

Agreement of the present results with earlier XPS data[14-16] on Fe, Co, Ni, and Cu is very good. Individual cases are discussed below.

B. Comparison with Theory

Let us compare these spectra with band-structure calculations and theoretical densities of states N(E). In doing so, we shall make the important assumption that the "density of ionization potentials", our measured I(E), does indeed resemble the density of energy eigenvalues N(E) as obtained from band-structure calculations. The implications of this assumption have been discussed elsewhere[14,22,27] and will not be repeated here. The real justification of this procedure until now has been derived from its success, notably in the almost one-to-one correspondence of N(E) and I(E) for semiconductors.[22] We shall follow this example here. At the same time, we note that any attempt to interpret I(E) in terms of N(E) may be regarded as a test for the applicability of the procedure.

The transition metal valence bands are derived from 3d and 4s atomic orbitals. The x-ray photoionization probabilities for these orbitals differ,[28] and the difference is conserved in the solid phase to the extent that Bloch states resemble the atomic wavefunctions near the nucleus, the region that determines the transition probability for $h\nu \sim 1500$ eV.[29,30] An estimate for the cross section ratio $\sigma(4s)/\sigma(3d)$ can be deduced from the areas under the sharp 3d peak (10 electrons) at $E_B \sim 10$ eV and the extensive 4s-derived valence region (2 electrons) at E_B between 10 eV and E_F in Zn (Fig. 3).

We obtain:

$$\frac{\sigma(4s)}{\sigma(3d)} = \frac{I(\text{"4s-band"})}{I(\text{"3d-peak"})} \cdot \frac{10}{2} = 1.3$$

This ratio will presumably increase somewhat in lighter elements, making the relative accentuation of s-derived bands in I(E) more pronounced. We will now compare the XPS spectra with theoretical results for each of the 3d metals.

1. Scandium and Titanium

Scandium and titanium start the 3d transition metal series with atomic configurations $3d^1 4s^2$ and $3d^2 4s^2$ respectively. They both crystallize in a hexagonal lattice with a c/a ratio of 1.59.

This structural identity introduces an element of rigidity into the band structure, which is borne out quite clearly in the high energy part of I(E), if we line up the peaks labeled B in I(E) for scandium and titanium (compare Fig. 1). Between peak B and the Fermi level E_F, I(E) rises in both elements to form a second peak. In scandium, E_F intersects I(E) before the peak is reached and the finite resolution moves the break in intensity to a point 0.4 eV below E_F. The titanium valence bands have to accommodate one more electron, and E_F is accordingly shifted up 0.5 eV. Thus the second peak A in the density of states is occupied beyond its maximum and E_F intersects a region of comparatively lower density with the break in I(E) again shifted down 0.4 eV due to finite resolution.

Toward lower energy, I(E) tails off in a superficially similar way for both metals. The bottom of the valence bands is, in each case, well marked by a distinctive kink E which occurs at $(E_F - 7.8)$ eV for Sc and at $(E_F - 8.1)$ eV for Ti. These points also coincide to within experimental error, if peak B is lined up in the two spectra.

A closer inspection reveals some important differences in detail. Between peak B and edge D, the scandium spectrum tails off in an s-like shape with an inflection point C around -3.8 eV. Beyond D, I(E) falls off to zero in a form resembling that of a free electron band. In titanium, we can just distinguish a discontinuity in slope marked C in Fig. 1.

The density of states N(E) for scandium and titanium has been calculated

by Altmann and Bradley[31,32] using the cellular method. We compare their results with our spectra in Fig. 5. The energies of characteristic features are set out in Table II.

The agreement in the overall shape of N(E) and I(E) is excellent for both metals. Notice especially the two peaks A and B and the change in position of E_F relative to peak A from scandium to titanium. The repeated changes in the curvature of I(E) between B and E in scandium as opposed to the essentially smooth decrease of I(E) in the same region in titanium agrees also quite well with the Altmann and Bradley calculation. The lack of resolution in their N(E) histograms however, makes the identification of feature C in the titanium spectrum difficult.

This quite satisfactory overall picture is marred by considerable discrepancies in the energies of characteristic features between N(E) and I(E), the exception being the total bandwidth of titanium (compare Table II). The different directions in which the upper and lower parts of N(E) deviate from their experimental counterparts reflect the different origins of these regions in terms of atomic orbitals. These differences make it somewhat arbitrary to match features C and D in I(E) for scandium with similar ones in N(E).

Mattheiss[33] has calculated the band structure of titanium along the Γ-K symmetry direction using the augmented plane wave method (APW). His total bandwidth of 6.3 eV falls considerably short of the 8.0 eV measured in this experiment. Hygh and Welch have also done several APW calculations on Ti. Their bandwidths also fall short of experiment but their density of states does show a two-peak structure.[34]

The APW bands calculated for Sc by Fleming and Loucks are likewise considerably narrower than observed.[35] S. G. Das et al.[36] have recently performed

an RAPW calculation on Sc. Their density of states compares qualitatively with our XPS results but again are much too narrow.

2. Vanadium and Chromium

Vanadium and chromium with 5 and 6 valence electrons, respectively, crystallize in the relatively open body-centered cubic (bcc) structure.

Chromium is an antiferromagnet at room teperature with a spin arrangement in the form of a spin-density wave. The wavelength of this spin-density wave is slightly less than twice the periodicity of the chemical lattice. Disregarding this difference, Asano and Yamashita[37] have treated the band structure of an idealized antiferromagnetic chromium by invoking the concept of a magnetic superlattice with twice the ordinary lattice constant. This reduces the Brillouin Zone (BZ) of the bcc lattice and introduces gaps of the order of 0.4 eV at points where bands cross the new zone boundaries. Though the occurrence of these gaps at the Fermi energy is essential for the stabilization of the antiferromagnetic order[38] in Cr, we do not expect them to alter the overall density of states strongly because they occur at different energies for different bands. This explains the great similarity in the densities of states derived by Connolly[39] from the band-structure calculation of paramagnetic and antiferromagnetic Cr by Asano and Yamashita.[37] It is therefore reasonable to compare our measurements with calculations on the paramagnetic state of bcc chromium. Densities of states N(E) have been calculated by several authors. The best qualitative and quantitative agreement between theory and experiment is found in the APW calculations by Gupta and Sinha,[40] as shown in Fig. 6. The two peaks at 2.0 and 3.9 eV in N(E) agree excellently in position and intensity with the corresponding peaks C and D in I(E). The edge at 4.9 eV in N(E) marks the position of the symmetry points H_{12} and N_1 and therefore the bottom of the d bands.

The peak closest to E_F in N(E) has two sharp spikes. The lower one at 2.4 eV arises from the flat bands connecting P_4 and N_2 along the P-N edge of the bcc Brillouin zone. The higher spike is not readily attributable to any particular regions in the BZ. The shoulder B is well reproduced in N(E) by a comparable shoulder at 0.8 eV. The edge of this shoulder toward E_F marks the position of Γ'_{25}. The region of very low electron density between this point in I(E) and the Fermi energy can be readily distinguished from the background and E_F itself is marked by a well-defined edge in I(E). The excellent agreement of I(E) and N(E) in this region provides dramatic confirmation of the essential correctness of the band structure calculation in predicting low values of N(E) near E_F. Neither the UPS nor the SXS spectra showed this feature.

A tail due mainly to a 4s-derived band extends down to 8.5 eV in N(E). This agrees reasonably well with the value 9.4±0.3 eV determined for the total valence bandwidth of chromium from our spectrum. The d-band densities of states calculated by Asdente and Friedel[41] using a tight-binding scheme agrees in general shape with our spectrum, as does the APW calculation of Snow and Waber.[42] Energies of symmetry points from four recent calculations[40,43,44] are compared with values deduced from our spectrum in Table III. It is clear from this Table that only the APW calculation of Gupta and Sinha[40] yields energies that agree with the XPS spectrum of chromium. This is surprising because the calculation was not self-consistent and it used an exchange parameter $\alpha = 1$. The tight-binding calculations[43,44] give bands that are generally too narrow. Furthermore they both give N(E) profiles that are definitely incompatible with our spectrum for the peak marked C in Fig. 6. For example, in both the N(E) calculated[39] from the band structure of Asano and Yamashita and in the N(E) given by Rath and Callaway, the splitting of peak A is 1.1 eV and the two parts are well

separated by a valley, a feature that would show up in the XPS spectrum. We must therefore conclude that the earlier interpretation[12] of structure on the UV photoemission ODS in terms of this density of states is not valid.

The valence-band spectrum of vanadium is very similar to that of chromium. Allowing for a shift in the Fermi level E_F due to the reduction by one in the number of valence electrons, we find a one-to-one correspondence in the characteristic features of the two spectra. In vanadium, E_F has moved down toward the higher peak by about 1 eV and the shoulder (B in Fig. 6) presumably lies above E_F. The separation between the two main peaks is slightly reduced from 1.8 eV in Cr to 1.6 eV in V. In addition, both peaks appear narrower. This reduction in d-band dispersion is presumably due to the slighly increased atomic spacing of vanadium as compared to chromium. In Fig. 6, we compare the Cr density of states of Gupta and Sinha,[40] shifted toward E_F, with our vanadium spectrum. Peak A marks the maximum near symmetry points P_4 and N_2. The energies of H_{12} and N_1 at the bottom of the d bands are well defined in the vanadium spectrum at (3.5 ± 0.3) eV below E_F.

The detailed picture that we have obtained for the density of states of Cr and V will aid us later in interpretation of the Fe spectrum.

3. Manganese

Manganese crystallizes in a distorted cubic lattice with 29 atoms per primitive cell. No band structure has therefore as yet been calculated. The VB-spectrum (see Fig. 2) shows a broad hump with a total width of 8.6 ± 0.3 eV. A peak A at $(E_F - 1.1)$eV and a shoulder B at $(E_F - 2.4)$eV can be distinguished in I(E). Judging from the steep slope at E_F, the density at E_F is probably close to its maximum value.

4. Copper and Zinc

Copper and zinc have closed 3d shells with atomic configurations $3d^{10}4s^1$ and $3d^{10}4s^2$ respectively. Copper crystallizes in a face centered cubic lattice and zinc in a hexagonal lattice.

The band structure of copper has been thoroughly studied, both theoretically and experimentally. Our spectrum agrees very well with earlier XPS work,[14-16] especially the high resolution spectrum of Hüfner, et al.[16] A comparison of our spectrum with a density of states obtained by Fong and Cohen[45] in a pseudopotential calculation allows the experimental determination of key energies (compare Fig. 7). The Fermi level intersects a region of low density derived from the remnants of the free-electron-like sp band. The steep rise at 2.0 eV in I(E) marks the top (X_5) of the completely filled d-bands. Two distinct peaks in N(E) around 2.2 eV and 3.4 eV are well reproduced in I(E) by a peak centered at 2.7 eV and a shoulder at 3.6 eV. The latter peak is derived from flat bands along $\Gamma \rightarrow L \rightarrow W$ and its maximum marks the position of Γ'_{25}.

A broader hump at 4.8 eV in N(E) derives its density from bands along the hexagonal edge W-K in the Brillouin zone of Cu. It finds its counterpart in a just visible shoulder at the same energy in I(E). The bottom of the d-bands is marked by the edge E in I(E) at $(E_F - 5.3 \pm 0.2)$ eV in excellent agreement with the 5.3 eV calculated by Fong and Cohen. Beyond the edge E, I(E) joins smoothly with the background of inelastically scattered electrons and it is not possible to assign an energy to Γ_1, the bottom of the valence bands from our spectrum. Krolikowski and Spicer[19] obtained a value for Γ_1 of 8.0 eV from their UPS data on Cu and Dobbyn et al.[5a] deduced a slightly higher value of 9.0 eV from the $M_{2,3}$ soft x-ray emission spectrum. We shall

therefore adopt an average value of 8.5 ± 0.5 eV for the position of Γ_1 below E_F.

Table IV compares the energies of certain symmetry points as obtained by the preceding analysis with some pertinent calculations, using X_5 as a fiducial point. The table is arranged to facilitate a comparison of the salient features in the band structure: the width of the d-bands ($X_5 - X_1$) and their position relative to the bottom of the sp band ($X_5 - \Gamma_1$). The latter is characterized by the energy separation $X_4' - \Gamma_1$ and the position of the Fermi level E_F relative to the bottom of the sp band Γ_1. $X_4' - \Gamma_1$ has been inferred from $X_5 - \Gamma_1$ (from our spectrum) and the energy of the optical transition $X_5 \rightarrow X_4'$ at 4.50 eV.[46] The close agreement between the experimental and all calculated values for the energies of the sp band (columns 2 and 3 in Table IV) is not surprising in view of the essentially free-electron-like character of the sp band that makes its shape insensitive to the potentials chosen in the calculation.

The parameters that characterize the width and position of the d bands varies considerably. The APW calculations by Chodrow[47] and Burdick[48] and the KKR calculation by Segall[49] employ the same potential and give consistent results in excellent agreement with experiment. Mattheiss'[33] APW band structure yields a width ($X_5 - X_1$) for the d-bands in good agreement with our value; the relative position is, however, high by about 1.4 eV.

The calculation by Segall[49] employing a ℓ-dependent potential improved the position of E_F and the d-bands relative to Γ_1 slightly, but yielded d bands about 0.8 eV too wide. The next two entries in Table IV are examples of self-

consistent calculations. A comparison of the results by Wakoh[50] (KKR) and Snow and Waber[42,51] (APW) employing the same full Slater exchange approximation illustrates the differences that can be encountered even in a self-consistent calculation. Whereas Wakoh's results agree excellently with our values, the $X_5 - X_1$ separation obtained by Snow is $\sim$ 0.7 eV too small and the position of X_5 is 1.5 eV too low. In the light of these results it is not too surprising that eigenvalues obtained from different starting potentials in non-self-consistent calculations show very substantial variations, as the next three entries in Table IV prove. It is interesting to note that the calculations, which give poor agreement with data relating to the Fermi surface, are the ones that disagree with our XPS results; namely the calculations by Snow[51] using full Slater exchange and the calculation by Ballinger and Marshall[52] employing a potential derived from Hermann-Skillman wavefunctions for atomic copper. This lends some additional support to our treating an eigenvalue spectrum as representative of a spectrum of ionization potentials. The last entry in Table IV is an example for an empirical pseudopotential band structure calculation using earlier UPS,[18] XPS,[14] and optical data[46] on Cu as input information for the proper choice of parameters. The agreement with experiment is excellent as expected.

Let us now turn to the valence bands of zinc. The Zn spectrum is shown on the right side of Fig. 3. We find an intense 3d peak (A in Fig. 3) centered at 10.18 ± 0.10 eV below E_F. The width of this peak is 1.45 ± 0.02 eV (full width at half maximum, FWHM). Emission from the 4s 4p bands is relatively less intense and extends from the well defined Fermi edge all the way down to the d-peak. The interference from the intense d-peak makes an accurate location of the bottom of the sp band impossible.

Recent UPS and SXS studies on Zn give values of 10.01(3) (UPS ref. 53)

and 10.36(15) (SXS ref. 54) for the position of the 3d emission relative to E_F that are in good agreement with our value. The higher resolution UPS results determine the spin-orbit splitting of the 3d peak in Zn to be 0.54 eV. Taking this splitting and a spectrometer resolution of 0.6 eV into account we deduced a component line width of not more than 0.8 eV from our spectrum. This sets an upper limit for the amount of energy dispersion in the d-bands of Zn, which is presumably even smaller since lifetime broadening of the 3d hole-states can well account for much of this width.

The picture that we have gained for the valence bands of Zn seems to favor the first-principles calculation of Juras et al.[55] employing the Green's function method over the results of Mattheiss'[33] APW calculation.

Juras et al. obtain an essentially free-electron-like sp band with a total occupied width of 10.6 eV and d-bands centered at $(E_F - 8.5)$ eV. The total width of the d-bands is about 1.6 eV. Mattheiss' calculation arrived at a seemingly unrealistic position of the d-bands about 7 eV below the bottom of the sp band.

Ley et al.[27] have discussed in detail the relationship between eigenvalue spectrum (band structure calculation) and the spectrum of ionization potentials as measured in photoelectron spectroscopy considering the relaxation screening of the hole-state by the passive electrons. On the basis of a simple model for the relaxation process, they arrive at the conclusion that the relaxation energy of the d-electrons in Zn is $\sim$ 5 eV bigger than that for the sp electrons. That would mean that the d-states lie about 5 eV below the bottom of the sp bands in the initial state which should be compared with the pertinent calculations. Thus the claim of Juras et al. that photoemission (and x-ray emission) experiments supported their results on the position of the d-bands may be wrong because relaxation effects must be accounted for.[27] The difference in relaxation

energy between sp and d-electrons is a consequence of the difference in the atomic origin of these electrons, which in Zn is rather undisturbed by hybridization.

This view is supported by the observation of Gelatt and Ehrenreich,[56] that the onset of optical transitions from the d bands in Au and Ag lies about a quarter of an eV higher than the corresponding energy separation between the top of the d bands and E_F in XPS data. The same holds for copper if we compare XPS data with the optical data of ref. 46.

Screening is presumably more important in the ionization process (XPS) than in the optical excitation. The difference in screening energy in the former is, however, greatly reduced in the noble metals as compared to Zn due to the considerable hybridization between d and sp bands. We take that as an indication that differential relaxation energies need not be considered for the interpretation of the remainder of the 3d transition metals.

5. Iron, Cobalt, and Nickel

Iron, cobalt, and nickel are ferromagnetic at room temperature. The ferromagnetism of these metals is regarded as itinerant in the sense that the d electrons, which are mainly responsible for the magnetic polarization, also participate in conduction.

The band model of ferromagnetism due to Stoner, Wohlfarth, and Slater (SWS)[57-58] features spin-polarized bands $\varepsilon_n(\vec{k})$ which are split by energies $\Delta E_n(\vec{k})$ due to the exchange interaction. ΔE is a function of wave vector $\vec{k}$ and band index n but it has usually been treated as a constant for d-derived bands and is set equal to zero for sp-derived bands. Estimates[59] for the average exchange splitting of the d bands ΔE are about 0.4 eV in Ni, 1.1 eV in Co, and 1.7 eV in Fe.

More recently band structure calculations of ferromagnetic Fe[60] and Ni[61] have derived the exchange splitting $E_n(k)$ self-consistently using an average Hartree-Fock field that is different for the two electron spin directions. These calculations reproduce the observed saturation moments quite satisfactorily.

Schemes different from the SWS-model have been proposed[62] which emphasize intra-atomic exchange and correlation effects in the formation of spin-ordered structures. However, to our knowledge no explicit calculations have been made which would bear directly on the electronic structure of ferromagnetic transition metals.

Two of the implications of the SWS model have been tested extensively:

(1) The spin polarization of electrons at the Fermi energy E_F is well established[63,64] and can be explained in sign and magnitude in the framework of the SWS model.[65]

(2) A number of spectroscopic techniques have been employed to study the changes in the band structure which are supposed to accompany the transition from the ferromagnetic to the paramagnetic state as ΔE goes to zero at the Curie temperature T_c.[66,69,5,7] The effects observed are however very small and do not readily lend themselves to a straightforward interpretation in terms of the SWS model.

In this inconclusive situation let us rephrase the question put forward by previous investigators from: "Does the band structure of a metal change according to the SWS-model if we cross the Curie temperature T_c?" to "Does the SWS-model give an appropriate description of the density of states N(E) of a ferromagnetic transition metal like iron below T_c?"

To do so, let us first consider the N(E) curve for chromium (Fig. 6) which we have found to be in excellent agreement with our XPS spectrum. Since

iron and chromium crystallize in the same bcc structure and have only slightly different lattice constants, we may regard this curve as a fair representation of N(E) for iron in the unmagnetized state. The Fermi energy E_F for this state would fall right at the top of the high density peak, as shown in Fig. 8a. The chemical potentials for spin up ($\lambda_\uparrow$) and spin down ($\lambda_\downarrow$) can easily be determined by allowing for the appropriate magnetic moment in ferromagnetic iron and assuming a rigid-band exchange splitting ΔE. In the final step, $\lambda_\uparrow$ and $\lambda_\downarrow$ coincide to form the new Fermi level in the SWS description of the ferromagnetic state. It is clear from Fig. 8b that this new density of states differs drastically from the nonpolarized N(E). Instead of a peak at E_F, we now have a region of very low electron density at E_F and a peak about 1.8 eV below E_F.

These two features are common to all N(E) calculations for Fe employing the SWS model and we find just these features in our XPS spectrum of iron, shown in Fig. 9 together with N(E) derived by Connolly[39] from the energy bands of Wakoh and Yamashita.[70]

The low intensity of I(E) at E_F and the position of peak A at $(E_F - 1.2)$ eV are not artifacts introduced by insufficient resolution. This becomes immediately clear from a comparison of the Fe spectrum with those of cobalt and nickel in Figs. 10 and 11, respectively.

The flat shoulder B in the spectrum of Fig. 9 finds its analog in a wide peak around $(E_F - 2.7)$ eV in Connolly's density of states. No such peak occurs in the density of states by Tawil and Callaway.[60] The bottom of the d bands is marked in both calculations by an edge in N(E) between 4.5 and 5.0 eV. Structure C in I(E) which presumably corresponds to this point lies at least 0.5 eV lower. The bottom of the valence bands is well marked at 9.8 eV by the intercept of the parabolic sp band with the baseline. The calculated values for the same point Γ_1 again fall short of this value by about 2.0 eV.

A very detailed treatment of the exchange problem in the band structure of ferromagnetic iron has been given by Duff and Das.[71] As a result they obtained significantly greater exchange splittings throughout the Brillouin zone as compared to other calculations. This increased the overall bandwidth to 13 eV and the d-bandwidth (point C in I(E)) to 9.9 eV, which both exceed the experimental values considerably. It is, however, clear from their calculation how assumptions about screening and the localizing effect of correlation influence the exchange and therefore the bandwidths. The input data provided by our spectra can give valuable information about the real magnitude of these many-body effects for the ferromagnetic state.

The valence-band spectra of cobalt and nickel are shown on Figs. 10 and 11. Cobalt shows two narrow peaks separated by 1.2 eV right at the Fermi level. The width of the d-bands is marked by the edge D at (E_F - 5.5) eV. The bottom of the valence bands is poorly defined because the tail joins smoothly into the background. We estimate a value of 9.5 ± 1.0 eV for the total bandwidth.

Densities of states N(E) of paramagnetic cobalt in its hcp structure have been calculated by Wong, Wohlfarth, and Hum,[72] and by Wakoh and Yamashita.[73] The former is based on a transformation of the Green's function method (KKR) into the form of an interpolation scheme. The latter calculation uses the KKR method self-consistently. The two densities of states are rather similar with two prominent peaks separated by $\sim$ 1.3 eV at the top of N(E) and a shoulder extending toward the bottom of the d-bands, some 4 to 5 eV below the top. The paramagnetic Fermi level intersects the top peak about halfway up the low energy edge.

The rigid exchange splitting ΔE was obtained in both calculations by allowing for the proper difference in spin-up and spin-down electrons. Values for ΔE are 1.35 eV (Ref. 72) and 1.71 eV (Ref. 73) respectively. These values

of ΔE would move the upper peak about 0.7 eV below E_F in the ferromagnetic state, a value slightly larger than the 0.5 eV observed in our spectrum. Wohlfarth[74] discussed ΔE in the light of several experimental data and arrived at a "best" value for ΔE (cobalt) of 1.1 ± 0.3 eV.

Shifting the N(E) curve of Ref. 73 rigidly by 1.1 eV gives excellent agreement with our data for structures A, C, D, and E, lending further support to SWS model for the ferromagnetic transition metals. The position of peak B is, however, off by $\sim$ 0.6 eV. This is not too surprising, since the forced reduction in ΔE necessarily gives a wrong magnetic moment in the original N(E). It appears that a reduction of the peak separation in the paramagnetic density of states together with a more realistic treatment of the exchange splitting would remedy both shortcomings.

The valence band spectrum of nickel is 8.9 ± 0.3 eV wide with a region of high density between E_F and (E_F - 4.0) eV, followed by a rather flat pedestal that turns toward the baseline at (E_F - 7.0) eV. The region of high density exhibits a peak A at 0.5 eV, an unresolved second peak B at 1.4 eV and on the trailing edge a shoulder at about 2.3 eV. Peak A is crucial in the interpretation of I(E) in terms of the numerous band structure calculations on ferromagnetic nickel.[75-81] All these calculations exhibit a peak in N(E) next to E_F, which arises from flat majority spin bands at the top of the d bands between symmetry points X and L in the BZ. The position of this peak relative to E_F depends on the exchange splitting at the top of the d bands, so that the lower limit in ΔE of $\sim$ 0.4 eV gives a position 0.3 eV below E_F and an upper limit in ΔE close to about 0.8 eV would move this peak to the position of peak A in I(E), 0.6 eV below E_F. This is quite in contrast to the position at (E_F - 0.3) eV accepted from UV photoemission data. We remind the reader however of the difficulties encountered in the interpretation of the UPS data

in terms of density of states (compare the variations in the positions of characteristic features observed at different excitation energies[82]). As a consequence we have strong indications that ΔE for nickel is between 0.7 and 0.8 eV for a region close to E_F.

In Fig. 11, we compare I(E) with the density of states obtained by J. Callaway and H. M. Zhang[78] even though their ΔE is 0.4 eV. The general features of this calculation agree, however, quite well with our spectrum: Peaks A and B and the bottom of the d bands (point D) are in almost quantitative agreement. From this figure, it seems reasonable to identify the pedestal around $E_F - 6.5$ eV in I(E) with emission from the sp bands at about the same energy in N(E).

Intensity considerations, however, make it likely that this feature can at least in part be attributed to a multielectron excitation associated with the photoemission from the 3d bands. Such a satellite is observed in the XPS spectrum of NiO[83] at a comparable energy below the d bands. We also find satellites associated with the 2p core levels in metallic nickel that are similar to those observed in NiO.[83]

Let us now return to the question put at the beginning of this section. "Is the SWS model appropriate to describe N(E) for ferromagnetic transition metals?" The answer is clearly yes from all we have seen in the interpretation of our XPS data. But why do the above mentioned experiments fail to detect the collapse of the exchange splitting above the Curie temperature? To qualify this question we have to consider two things: what has been measured and what does "above T_c" mean. Above T_c means in all these cases not more than 1.07 T_c. And the quantity measured was closely related to the density of states, which is well known to be already quite well developed for clusters of only 10 to 20 atoms.

The negative results of these experiments then mean that at 1.07 T_c

there is still a nonvanishing spin density over a region covering a cluster of atoms. This is quite compatible with the loss of any long-range spin order and with the nature of the magnetic transition as a second-order transition.

V. MULTIPLET SPLITTING OF 3s CORE LEVELS

The phenomenon of multiplet splitting of core-level binding energies is well-known in the XPS spectra of transition metal halides and oxides. It arises because the hole produced by photoemission can couple either parallel or antiparallel to the majority 3d spin of the ion, producing final states of different energy. The simplest description of the splitting is obtained by neglecting electron-electron correlation and using Van Vleck's theorem[84] which yields for the 3s splitting

$$\Delta E(3s) = \frac{(2S_i + 1)}{5} G^2(3s,3d)$$

where S_i is the initial-state spin. In fact, electronic correlation effects are in general not negligible. This tends to reduce the splitting from the above value and produce satellite peaks.

Despite these not-easily-calculable many-body effects, multiplet splitting has some advantages in comparison with other methods. Magnetic susceptibility can be measured quite accurately and can yield valuable information on the existence or nonexistence of localized moments. Its disadvantage lies in the more complicated systems, in which one cannot be sure *a priori* that all the ions are magnetically equivalent. In these cases, the observed average atom moment could reflect either a well-defined moment present on every atom or a wide distribution of moments with this average value. Neutron diffraction is another powerful technique, particularly for the study of antiferromagnetically ordered states, in which extra magnetic periodicity gives rise to well-defined diffraction features. By analysis of the structure and form factors associated with the magnetic scattering, it is possible to study both the magnitude and relative orientation of the spins.

Above the transition temperature, one can measure only diffuse magnetic scattering. From the magnitude of this background an average moment can be calculated. The difficulty arises from the fact that neutron scattering is a relatively slow process, with a typical interaction time of $\sim 10^{-12}$ sec. Thus if the fluctuation time of the moments is much faster than 10^{-12} sec, the analysis could yield a spurious zero result. X-ray photoemission, however, is a fast process occuring on a timescale of $\sim 10^{-16}$ sec, and is certainly faster than any spin fluctuation time. In addition XPS, being a spectroscopic technique, can distinguish between single-valued moment systems and distributions of moments by the number and widths of the photoemission lines.

An excellent example of the complementary nature of these techniques is provided by α-Mn.[85] Below T_N ($\sim$ 100°K), neutron diffraction provided a reasonable picture of the moment structure, despite the inherent complexity of a crystal with 29 atoms per primitive cell. Above T_N, magnetic diffuse scattering yielded an upper limit of 0.5 μ_B for the magnetic moment per atom.[86] This result was shown to be spurious by the susceptibility measurement of Nagasawa and Vehinami[87] who derived a value of 2.37(7) μ_B/atom. This was confirmed by the XPS measurements which, using a Van Vleck's theorem treatment, yielded a value of $\sim$ 2.5 μ_B/atom. In addition, the appearence of two sharp lines in the spectrum provided strong evidence that all the atoms in the crystal carried moments close to this value.

In the 3d transition series, one can distinguish three distinct classes of magnetic behavior, "normal" Pauli-type paramagnetism in which the susceptibility is only weakly temperature dependent, antiferromagnetism, and ferromagnetism. Scandium, titanium and vanadium comprise the first class, manganese and chromium the second, and iron, cobalt and nickel the third. We shall consider

each of these classes in turn.

A. Scandium, Titanium and Vanadium.

In a sense, Sc, Ti, and V exhibit the solid-state effects on the 3s spectra most strongly. A free atom or dipositive ion of any of these elements would be expected to show detectable multiplet splitting; however in the solid this splitting disappears. As can be seen in Fig. 12, the 3s spectra appear as single, rather broad lines. They are somewhat asymmetric, but this feature is generally found in photoemission spectra of core levels in metals. It arises from the self-consistent screening of the final (core hole) state by the valence electrons.[88]

The absence of multiplet splitting in these metals is consistent with the picture of itinerant 3d electrons well described by one-electron band theory. In this picture a paramagnetic metal is described as having spin-up and spin-down bands equally populated, with no resultant spin density at any site. This lack of unpaired spin density is reflected in the absence of multiplet splitting in these metals. This picture is further borne out by the magnetic susceptibility measurements on these metals,[89] which show no strong temperature dependence.

B. Chromium and Manganese

Chromium and manganese are both antiferromagnetic, but their magnetic structures differ in one important way. Below T_N(310°K) the magnetic periodicity of Cr is incommensurate with the lattice periodicity,[90] with the result that the local spin densities at crystallographically equivalent sites are unequal. As a result, the antiferromagnetism in Cr has been described as a collective phenomenon of the itinerant valence electrons, resulting from the peculiar "nesting"

properties of the Fermi surface.[91] In the case of Mn no such "periodicity mismatch" was observed.[92]

While the Mn results are straightforward and amenable to a Van Vleck's theorem type of analysis, the chromium results suffer from an unfortunate experimental ambiguity. Because the Neel temperature of 310°K is so close to room temperature, we cannot be sure whether the surface of our sample, under intense x-ray bombardment, was above or below T_N. Below T_N neutron diffraction[93] has shown that the sinusoidal modulation of the atomic moments has a periodicity 27 times that of the unit cell at T_N, and that the maximum in the magnetic moment distribution corresponds to $\sim .59\ \mu_B$. Above the Neel temperature, incoherent neutron scattering detected no component of any random moment fluctuating with a frequency less than ~ 0.1 eV/$\hbar$. However, spin-density-wave theory would predict spin fluctuations at a frequency characteristic of the d-bandwidth $\sim$ 4 eV/$\hbar$, too fast to be detected by neutron scattering.

The photoemission spectrum of the Cr 3s region as shown in Fig. 13 reveals a broad structure of two peaks separated by 2.8 eV. If one takes the simplistic Van Vleck's theorem approach and derives $(2S_i + 1)$ from the 3s splitting in CrF_3, it appears that the splitting in Cr metal corresponds to a moment of $\sim 1.7\ \mu_B$/atom. As our measurement was probably performed on Cr above T_N, due to intense x-ray bombardment of the sample, this result bears an interesting similarity to that in Mn. In both cases the simple analysis suggests that the moments in the paramagnetic phase are considerably larger than they are in the antiferromagnetic phase. The widths of the individual components of the Cr spectrum are considerably larger than in Mn, perhaps reflecting a distribution of moments in Cr. At this time it is, however, impossible to state anything quantitative. It would be useful to measure both the splitting and linewidth

as a function of temperature starting well below T_N and continuing well past it.

C. Iron, Cobalt, and Nickel

Iron, cobalt, and nickel are all ferromagnetic at room temperature, exhibiting a macroscopic magnetic moment. The 3s spectra thus is expected to show multiplet splitting. In Fig. 14, considerable structure is indeed apparent in the 3s photoemission spectrum. There is, however, a striking difference between the appearance of these spectra and those of Cr and Mn. In Cr and Mn, the spectrum was clearly composed of two fairly well defined peaks of comparable linewidth, while if the ferromagnetic spectra were regarded as being composed of two lines, the low-spin component would have 2-3 times the width of the high-spin component. This effect is unlikely to arise from a distribution of moments, as in that case the high spin peak would be equally broadened. It could be suggested that this effect results from excess life time broadening of the low-spin hole state. This could be rationalized on the basis that there is an excess of "spin up" electrons in the ferromagnetic state, which can fill the 3s hole without flipping spins. There are, however, two factors which argue against this; (1) the lines are not clearly Lorentzian in shape, and life-time broadening is always Lorentzian, and (2) Fadley and Shirley[23] studied the 3s spectrum of iron below and above the Curie point, and while their spectra were of lower resolution they would have detected any dramatic decrease in broadening for $T > T_c$, and none was observed. We are thus led to conclude that the width of this structure arises from correlation effects.

Correlation effects are well known to cause dramatic effects in XPS core-level multiplet splitting experiments. In addition to reducing splittings by a factor of two from Hartree-Fock estimates, configuration interaction in the final state can produce low-spin satellite peaks of appreciable intensity, as in

the case of MnF_2.[24] It is not unreasonable to assume that in a metal, where there exists a continuum of one-electron orbitals of strongly mixed angular momentum, strong interconfiguration mixing could produce a quasicontinuum of final states. That strong interconfiguration mixing should be present in a ferromagnetic metal is furthermore quite plausible, as single determinantal theories are quite unsatisfactory for the description of ferromagnetic states (e.g., they cannot explain spin-waves, while theories involving linear combinations of determinants can).[94]

Figure 15 shows Cu and Zn 3s spectra. These metals have filled 3d shells and low values of N(E) at E_F. Their 3s XPS lines show no indication of multiplet splitting.

ACKNOWLEDGMENTS

We would like to thank Professor G. Somorjai for the gift of Cr, V, and Cu single crystals and Dr. H. Nadler for the gift of a Ti single crystal.

FOOTNOTES AND REFERENCES

*Work performed under the auspices of the U. S. Atomic Energy Commission.

†IBM Fellow.

1. L. Hodges, R. E. Watson, and H. Ehrenreich, Phys. Rev. B 5, 3953 (1972).

2. For a review see C. Herring, Magnetism, ed. by G. T. Rado and H. Suhl (Academic Press, New York, 1966), Vol. IV.

3. D. W. Fischer, J. Appl. Phys. 40, 4151 (1969).

4. D. W. Fischer, Phys. Rev. B 4, 1778 (1971).

5.a) R. C. Dobbyn, M. L. Williams, J. R. Cuthill, and A. J. McAlister, Phys. Rev. B 2, 1563 (1970).

b) A. J. McAlister, J. R. Cuthill, R. C. Dobbyn, M. L. Williams, and R. E. Watson, Phys. Rev. Letters 29, 179 (1972).

6. D. W. Fischer and W. L. Baun, J. Appl. Phys. 39, 4757 (1968).

7. D. T. Pierce and W. E. Spicer, Phys. Rev. Letters 25, 581 (1970).

8. C. N. Berglund and W. E. Spicer, Phys. Rev. 136, A1030 (1964); 136, A1044 (1964).

9. A. J. Blodgett Jr. and W. E. Spicer, Phys. Rev. 146, 390 (1966).

10. A. Y.-C. Yu and W. E. Spicer, Phys. Rev. Letters 23, 1171 (1966).

11. A. J. Blodgett and W. E. Spicer, Phys. Rev. 158, 514 (1967).

12. D. E. Eastman, J. Appl. Phys. 40, 1387 (1969).

13. D. E. Eastman, Sol. St. Comm. 7, 1697 (1969);
D. E. Eastman, Electron Spectroscopy, ed. by D. A. Shirley (North-Holland Publishing Co., Amsterdam, 1972), p. 487.

14. C. S. Fadley and D. A. Shirley, Electronic Density of States, Nat. Bur. Std. (U.S.A.) Special Publication 323, 163 (1971).

15. I. Lindau and L. Wilson, Phys. Letters 42A, 279 (1972).

16. S. Hüfner, G. K. Wertheim, and J. H. Wernick, Phys. Rev. B8, 4511 (1973).

17. G. D. Mahan, Phys. Rev. 163, 612 (1967);
C. Kunz, R. Haensel, G. Keitel, P. Schreiber, and B. Sonntag, Electronic Density of States, Nat. Bur. Std. (U.S.A.) Special Publication 323, 253 (1971).

18. See e.g., W. E. Spicer, in Electronic Density of States, Nat. Bur. Std. Special Publication 323, 139, 191 (1971).

19. See e.g., W. F. Krolikowski and W. E. Spicer, Phys. Rev. 185, 882 (1969).

20. N. V. Smith, Electronic Density of States, Nat. Bur. Std. Special Publication 323, 191 (1971).

21. D. E. Eastman and W. D. Grobman, Phys. Rev. Letters 28, 1327 (1972).

22. L. Ley, R. A. Pollak, F. R. McFeely, S. P. Kowalczyk, and D. A. Shirley, Phys. Rev. B 9, 600 (1974).

23. C. S. Fadley and D. A. Shirley, Phys. Rev. A 2, 1109 (1970).

24. S. P. Kowalczyk, L. Ley, R. A. Pollak, F. R. McFeely, and D. A. Shirley, Phys. Rev. B 7, 4009 (1973).

25. R. A. Pollak, S. P. Kowalczyk, L. Ley, and D. A. Shirley, Phys. Rev. Letters 29, 274 (1972).

26. T. E. Madey, J. T. Yates, and N. E. Erickson, Chem. Phys. Letters 19, 487 (1973).

27. L. Ley, S. P. Kowalczyk, F. R. McFeely, R. A. Pollak, and D. A. Shirley, Phys. Rev. B 8, 2392 (1973).

28. U. Gelius, Electron Spectroscopy, ed. by D. A. Shirley (North-Holland Publishing Co., Amsterdam, 1972), p. 311.

29. R. G. Cavell, S. P. Kowalczyk, L. Ley, R. A. Pollak, B. Mills, D. A. Shirley, and W. Perry, Phys. Rev. B 7, 5313 (1973).

30. F. R. McFeely, S. P. Kowalczyk, L. Ley, R. G. Cavell, R. A. Pollak, and D. A. Shirley, Phys. Rev. B 9, 5268 (1974).

31. S. L. Altmann and C. J. Bradley, Proc. Phys. Soc. (London) 92, 764 (1967).

32. S. L. Altmann and C. J. Bradley, Soft X-Ray Band Spectra, ed. by D. J. Fabian (Academic Press, New York, 1968), p. 265.

33. L. F. Mattheiss, Phys. Rev. 134, A970 (1964).

34. E. H. Hygh and R. M. Welch, Phys. Rev. B 1, 2424 (1970); R. M. Welch and E. H. Hygh, Phys. Rev. B 4, 4261 (1971); R. M. Welch and E. H. Hygh, Phys. Rev. B 9, 1993 (1974).

35. G. S. Fleming and T. L. Loucks, Phys. Rev. 173, 685 (1968).

36. S. G. Das, A. J. Freeman, D. D. Koelling, and F. M. Mueller, Magnetism and Magnetic Materials - 1972, ed. by C. D. Graham Jr. and J. J. Rhyne (American Institute of Physics, New York, 1973), p. 1304.

37. S. Asano and J. Yamashita, J. Phys. Soc. (Japan) 23, 714 (1967).

38. W. M. Lomer, in Proc. Int. School of Physics, E. Fermi, Course XXXVII, ed. by W. Marshall (Academic Press, New York, 1967).

39. J. W. D. Connolly, Electronic Density of States, Nat. Bur. Std. Special Publication 323, 27 (1971).

40. R. P. Gupta and S. K. Sinha, Phys. Rev. B 3, 2401 (1971).

41. M. Asdente and J. Friedel, Phys. Rev. 124, 384 (1961).

42. E. C. Snow and J. T. Waber, Acta Metall. 17, 623 (1969).

43. M. Yasin, E. Hayashi, and M. Shimiga, J. Phys. Soc. Japan 29, 1440 (1970).

44. J. Rath and J. Callaway, Phys. Rev. B 8, 5398 (1973).

45. C. Y. Fong and M. L. Cohen, Phys. Rev. Letters 24, 306 (1970).

46. B. R. Cooper, H. Ehrenreich, and H. R. Philipp, Phys. Rev. 138, A494 (1965).

47. M. Chodrow, Phys. Rev. 55, 675 (1939).

48. G. A. Burdick, Phys. Rev. 129, 138 (1963).

49. B. Segall, Phys. Rev. 125, 109 (1962).

50. S. Wakoh, J. Phys. Soc. (Japan) 20, 1894 (1965).

51. E. C. Snow, Phys. Rev. 171, 785 (1968).

52. R. A. Ballinger and C. A. W. Marshall, Proc. Phys. Soc. (London) 91, 203 (1967).

53. A. D. McLachlan, J. G. Jenkin, J. Liesegang, and R. C. Leckey, J. Electr. Spectr. 3, 207 (1974).

54. S. Hanzely and R. J. Liefeld, Electronic Density of States, Nat. Bur. Std. Special Publication 323, 319 (1971); recalculated from L_α with our value of 1021.96(15) eV for the $2p_{3/2}$ binding energy relative to E_F.

55. G. E. Juras, B. Segall, and C. B. Sommers, Sol. St. Comm. 10, 427 (1972).

56. C. D. Gelatt, Jr. and H. Ehrenreich, Phys. Rev. B10, 398 (1974).

57. E. C. Stoner, Phil. Mag. 15, 1018 (1933); E. P. Wohlfarth, Rev.Mod.Phys. 25, 211 (1953).

58. J. C. Slater, Phys. Rev. 49, 537, 931 (1936).

59. E. P. Wohlfarth, Proc. Int. Conf. Magnetism (Institute of Physics and Physical Society of London, Nottingham, England, 1965), p. 51.

60. R. A. Tawil and J. Callaway, Phys. Rev. B 7, 1242 (1973).

61. J. Callaway and C. S. Wang, Phys. Rev. B 7, 1096 (1973).

62. See e.g., J. H. Van Vleck, Rev. Mod. Phys. 25, 220 (1953).

63. U. Banninger, G. Bush, M. Campagna, and H. C. Siegmann, Phys. Rev. Letters 25, 585 (1970).

64. W. Gluich, G. Regenfus, and R. Siegmann, Phys. Rev. Letters 27, 1066 (1971).

65. B. A. Politzer and P. H. Cutler, Phys. Rev. Letters 28, 1330 (1972).

66. C. S. Fadley and D. A. Shirley, Phys. Rev. Letters 21, 980 (1968).

67. G. P. Pells and M. Shiga, J. Phys. C 2, 1835 (1969).

68. B. Hinnann and J. Hölzl, Phys. Rev. Letters 26, 1573 (1971).

69. J. E. Rowe and J. C. Tracy, Phys. Rev. Letters 27, 799 (1971).

70. S. Wakoh and J. Yamashita, J. Phys. Soc. (Japan) 21, 1712 (1966).

71. K. J. Duff and T. P. Das, Phys. Rev. B 3, 192 (1971).

72. K. C. Wong, E. P. Wohlfarth, and D. M. Hum, Phys. Letters 29A, 452 (1969).

73. S. Wakoh and J. Yamashita, J. Phys. Soc. (Japan) 28, 1151 (1970).

74. E. P. Wohlfarth, J. Appl. Phys. 41, 1205 (1970).

75. S. Wakoh, J. Phys. Soc. (Japan) 20, 1894 (1965).

76. E. D. Thompson and J. J. Myers, Phys. Rev. 153, 574 (1967).

77. J. W. D. Connolly, Phys. Rev. 159, 415 (1967).

78. J. Callaway and H. M. Zhang, Phys. Rev. B 1, 305 (1970).

79. E. I. Zornberg, Phys. Rev. B 1, 244 (1970).

80. J. Langlinais and J. Callaway, Phys. Rev. B 5, 124 (1972).

81. J. Callaway and C. S. Wang, Phys. Rev. B 7, 1096 (1973).

82. D. E. Eastman, J. Phys. (France) C1 32, 293 (1971).

83. K. S. Kim, Chem, Phys. Letters 26, 234 (1974) and references therein.

84. J. H. Van Vleck, Phys. Rev. 46, 405 (1934).

85. F. R. McFeely, S. P. Kowalczyk, L. Ley, and D. A. Shirley, Sol. St. Comm., (to be published)

86. C. G. Shull and M. K. Wilkinson, Rev. Mod. Phys. 23, 100 (1953).

87. H. Nagasawa and M. Uchinami, Phys. Letters 42A, 463 (1973).

88. L. Ley, F. R. McFeely, S. P. Kowalczyk, J. Jenkin and D. A. Shirley, Phys. Rev. B (to be published).

89. E. W. Collins and P. C. Gehlen, J. Phys. F 1, 908 (1971); B. G. Childs, W. E. Gardner and J. Penfold, Phil. Mag. 5, 1257 (1960).

90. G. E. Bacon, Acta. Cryst. 14, 823 (1961).

91. W. M. Lomer, Proc. Phys. Soc (London) 80, 489 (1962).

92. T. Yamada, N. Kouitomi, Y. Nakai, D. E. Cox and G. Shirane, J. Phys. Soc. (Japan) 28, 615 (1970).

93. M. K. Wilkinson, E. O. Wollun, W. C. Koehler and J. W. Cable, Phys. Rev. 127, 2080 (1962). See also Ref. 2, p. 326.

94. Ref. 2, p. 125-127.

Table I. Energies of characteristic features in the valence band spectra of the transition metals. Errors are given parenthetically. Entries are in eV.

Element	A	B	C	D	E
Sc	0.4(1)	1.2(1)	3.8(3)	5.3(2)	7.8(2)
Ti	0.8(1)	1.7(2)	4.2(2)	-	8.1(2)
V	0.7(1)	2.3(1)	5.1(3)	-	9.0(2)
Cr	0.6(1)	1.3(1)	2.3(1)	4.1(1)	9.4(3)
Mn	1.1(1)	2.4(2)	-	-	8.6(3)
Fe	1.2(1)	2.9(1)	5.5(5)	-	9.8(2)
Co	0.5(1)	1.7(1)	3.8(3)	5.5(1)	9.5(1.0)
Ni	0.5(1)	1.4(1) ($B' = 2.0$)	3.5(2)	4.6(3)	8.9(3)
Cu	2.0(1)	2.7(1)	3.6(2)	4.6(2)	5.3(2)
Zn	10.2(1)	-	-	-	-

Table II. A comparison of structural features in the valence band spectrum of scandium and titanium with the corresponding densities of states calculated by Altmann and Bradley.[31,32] The entries are in eV below the Fermi energy E_F. Errors are given parenthetically.

	Sc		Ti	
	Expt.	Theory	Expt.	Theory
E_F	0	0	0	0
peak A	0.41(1)	0.0	0.8(1)	1.0
peak B	1.2(1)	1.7	1.7(2)	3.4
inflection point C	3.8(3)	2.4	4.2(2)	-
inflection point D	5.3(3)	3.6[a]	-	-
bottom of VB E	7.8(2)	6.0	8.1(2)	8.0

[a]The identification of features C and D in N(E) is ambiguous (see text).

Table III. Energies of symmetry points in the valence bands of chromium (eV below E_F).

Symmetry Point	Tight-binding plus OPW[a]		Tight-binding, SCF[b]	APW,	Expt., this work
	$\alpha = 1$	$\alpha = 0.725$	$\alpha = 2/3$	$\alpha = 1$[c]	
Γ'_{25}	1.0	1.0	1.0	0.7	0.8(1)
P_4	1.6	2.0	2.2	2.5	2.9(2)
N_2	2.3	2.4	2.7	2.4	
H_{12}	3.0	3.3	4.0	4.8	4.8(3)
N_1	3.3	3.9	4.3	4.9	
Γ_1	5.1	6.9	5.9	8.7	9.4(3)

[a] Ref. 43. Here α is the exchange parameter

[b] Ref. 44.

[c] Ref. 40.

Table IV. Characteristic energy differences in the valence bands of copper. Values are given in eV, and errors are given parenthetically.

	$X_4' - \Gamma_1$	$E_F - \Gamma_1$	$X_5 - \Gamma_1$	$X_5 - X_1$	$X_5 - \Gamma_{25}'$
Experiment	11.0(5)[a]	8.5(5)[b]	6.5(5)	3.3(3)	1.6(2)
Theory					
APW, Chodrow Ref. 47	11.2	--	7.0	3.2	1.7
APW, Burdick Ref. 48	10.9	8.8	7.0	3.4	1.5
KKR, Segall Ref. 49	11.1	9.0	7.0	3.5	1.6
KKR, Segall Ref. 49 ℓ-dependent potential	11.0	8.9	6.4	4.1	1.9
Mattheiss, Ref. 33	12.4	--	7.9	3.5	1.5
Wakoh, Ref. 50 self-consistent	--	8.8	6.8	3.3	1.5
Snow, Ref. 51 self-consistent	10.8	8.3	5.0	2.6	1.2
Ballinger and Marshall Ref. 52 (Hermann-Skillman)	8.7	8.0	4.2	2.4	1.2
Ballinger and Marshall Ref. 52, 2/5 Gaspar	11.0	9.0	6.5	3.7	1.9
O'Sullivan et al. Ref. c	11.5	8.9	7.0	3.2	1.4
Fong and Cohen Ref. 45	10.8	8.5	6.7	3.3	1.8

[a] Deduced using the value of 4.5 eV obtained for $X_4' - X_5$ from optical data (Ref. 46) and the value for $(X_5 - \Gamma_1) = 6.5$ eV.

[b] Average value from Ref. 19 and Ref. 5a.

[c] W. J. O'Sullivan, A. C. Switendick, and J. E. Schirber, Phys. Rev. B 1, 1443 (1970).

FIGURE CAPTIONS

Fig. 1. X-ray photoemission spectrum I(E) of the valence band region of Sc, Ti, V, and Cr. The background contribution due to inelastically scattered electrons has been subtracted. The features denoted by letters are discussed in the text and the energies are given in Table I.

Fig. 2. X-ray photoemission spectrum I(E) of the valence band region of Mn, Fe, Co, and Ni. The background contribution due to inelastically scattered electrons has been subtracted. The features denoted by letters are discussed in the text and the energies are given in Table I.

Fig. 3. X-ray photoemission spectrum I(E) of the valence band region of Cu and Zn. The background due to inelastically scattered electrons has been subtracted. The features denoted by letters are discussed in the text and the energies are given in Table I.

Fig. 4. A comparison of the valence band spectra of Cr obtained by ultraviolet photoemission (UPS, Ref. 12), soft x-ray spectroscopy (SXS, Ref. 4) and x-ray photoemission (XPS, this work).

Fig. 5. A comparison of the x-ray photoemission valence band spectra I(E) (upper curves) with density of states N(E) (lower curves) calculated by Altmann and Bradley (Ref. 31 and 32) for Sc and Ti. The energies of the characteristic features are given in Table II.

Fig. 6. The x-ray photoemission valence band spectra I(E) of V and Cr are compared with the APW results of Gupta and Sinha (Ref. 40). For V we have used Gupta and Sinha's Cr density of states with the Fermi level shifted corresponding to the reduction by one of the number of valence electrons.

Fig. 7. The x-ray photoemission valence band spectrum I(E) of Cu is compared with the density of states N(E) of Fong and Cohen (Ref. 45). A comparison of the energy of features of I(E) with theory is given in Table IV.

Fig. 8.a) The bcc chromium density of states of Ref. 40 $\lambda_{\downarrow}$ and $\lambda_{\uparrow}$, the spin up and spin down chemical potentials for bcc Fe are determined from the magnetic moment of Fe under the assumption of a rigid band exchange splitting.

b) The resulting spin-polarized density of states where the chemical potentials $\lambda_{\downarrow}$ and $\lambda_{\uparrow}$ have been made to coincide. This density of states should be representative for that of ferromagnetic iron.

Fig. 9. A comparison of the x-ray photoemission valence band spectrum I(E) of Fe (upper curve) with the N(E) derived by Connolly (Ref. 39) (lower curve).

Fig. 10. The x-ray photoemission valence band spectrum of Co is compared with the density of states calculated by Wong et al. (Ref. 72) (middle curve) and by Wakoh and Yamashita (Ref. 73) (histogram).

Fig. 11. A comparison of the x-ray photoemission valence band spectrum I(E) of Ni (upper curve) with the calculated density of states obtained by Callaway and Zhang (Ref. 78) (lower curve).

Fig. 12. The 3s spectra of Sc, Ti and V.

Fig. 13. The 3s spectra of Cr and Mn.

Fig. 14. The 3s spectra of Fe, Co and Ni.

Fig. 15. The 3s spectra of Cu and Zn.

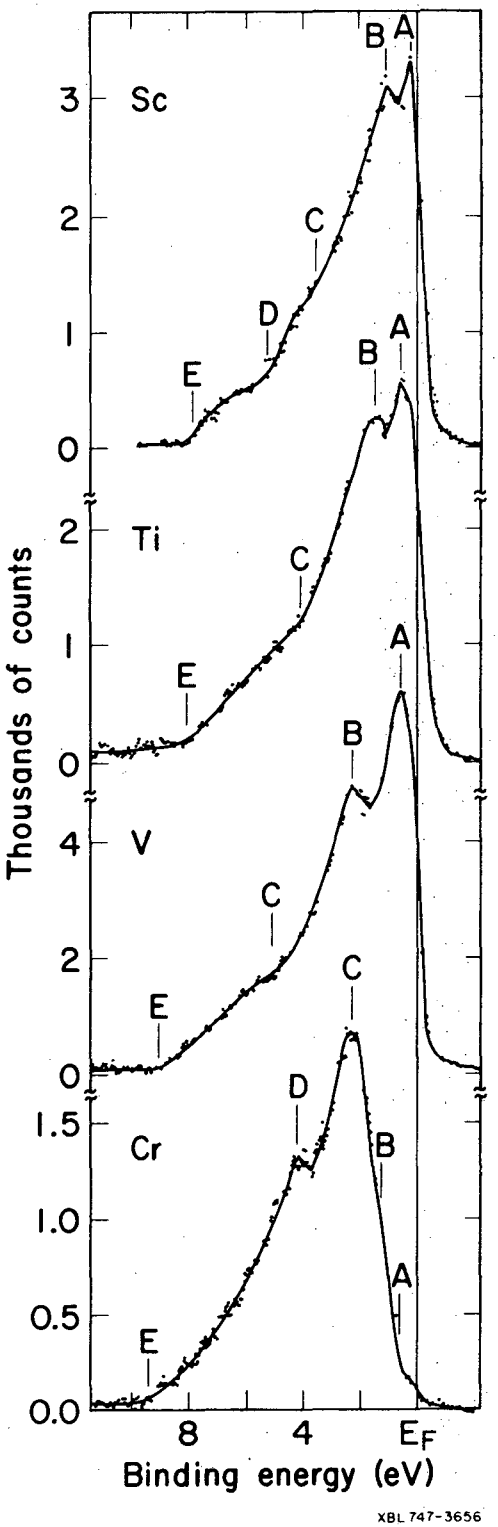
Sc
Ti
V
Cr
A
B
C
D
E
Thousands of counts
3
2
1
0
4
1.5
1.0
0.5
0.0
8
4
E_F
Binding energy (eV)
XBL 747-3656

Fig. 1

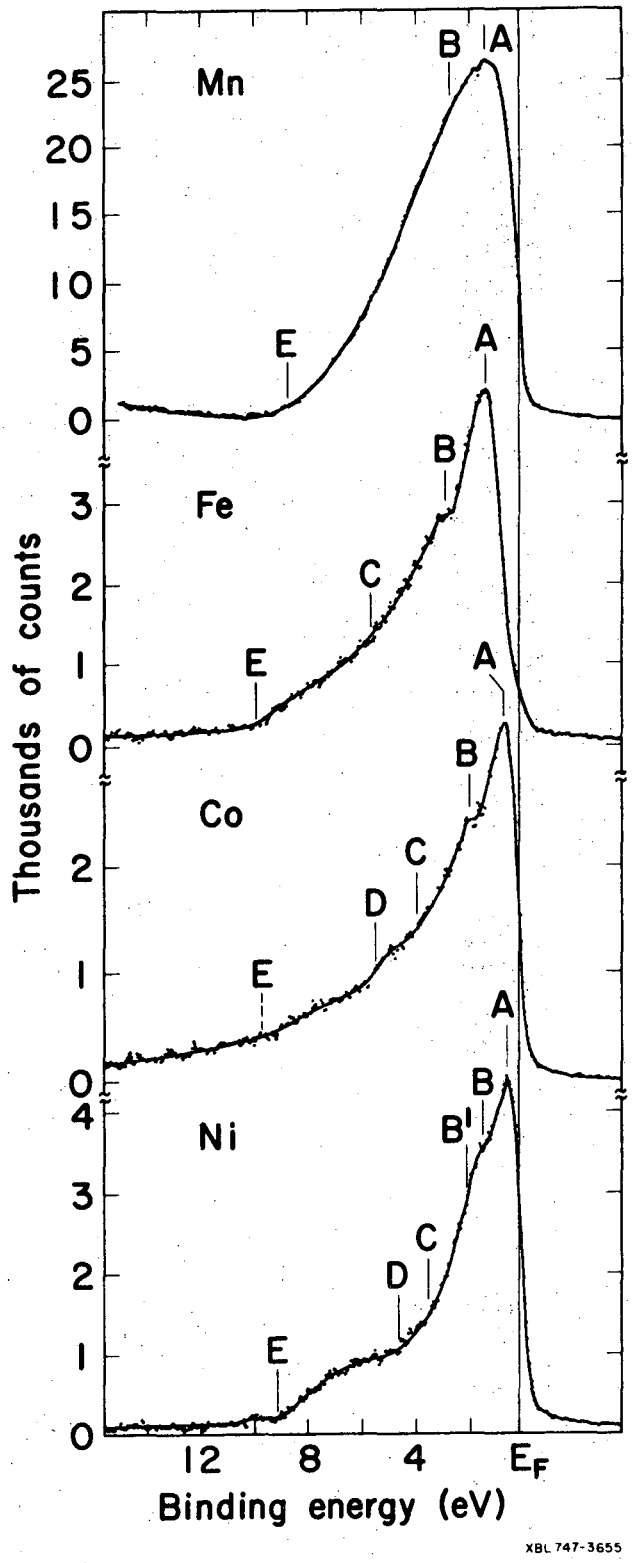
Mn
Fe
Co
Ni
A
B
B'
C
D
E
Thousands of counts
Binding energy (eV)
12
8
4
E_F
XBL 747-3655

Fig. 2

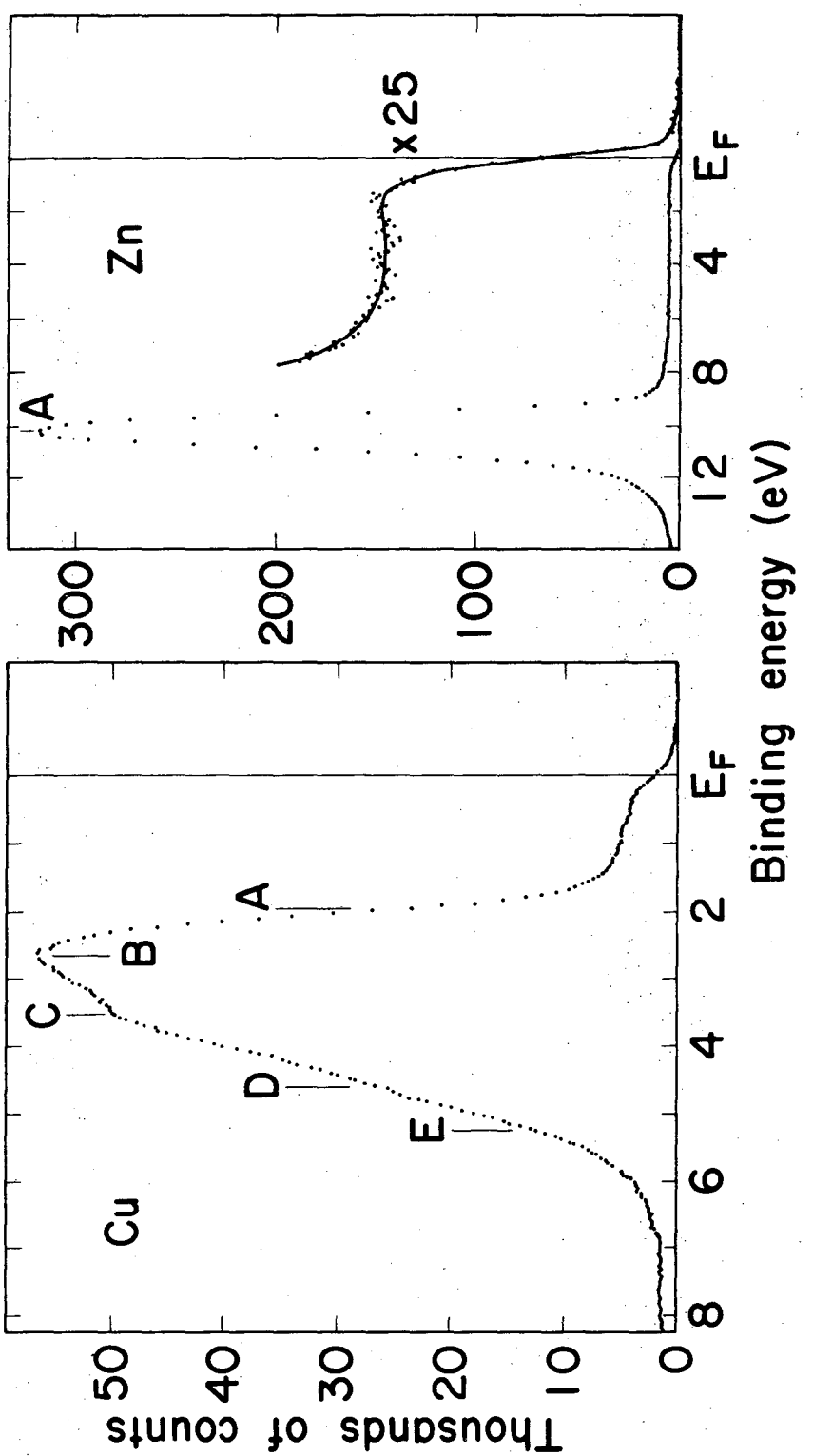
Thousands of counts
Cu
A
B
C
D
E
E_F
Zn
x25
A
E_F
Binding energy (eV)
XBL 747-3654

Fig. 3

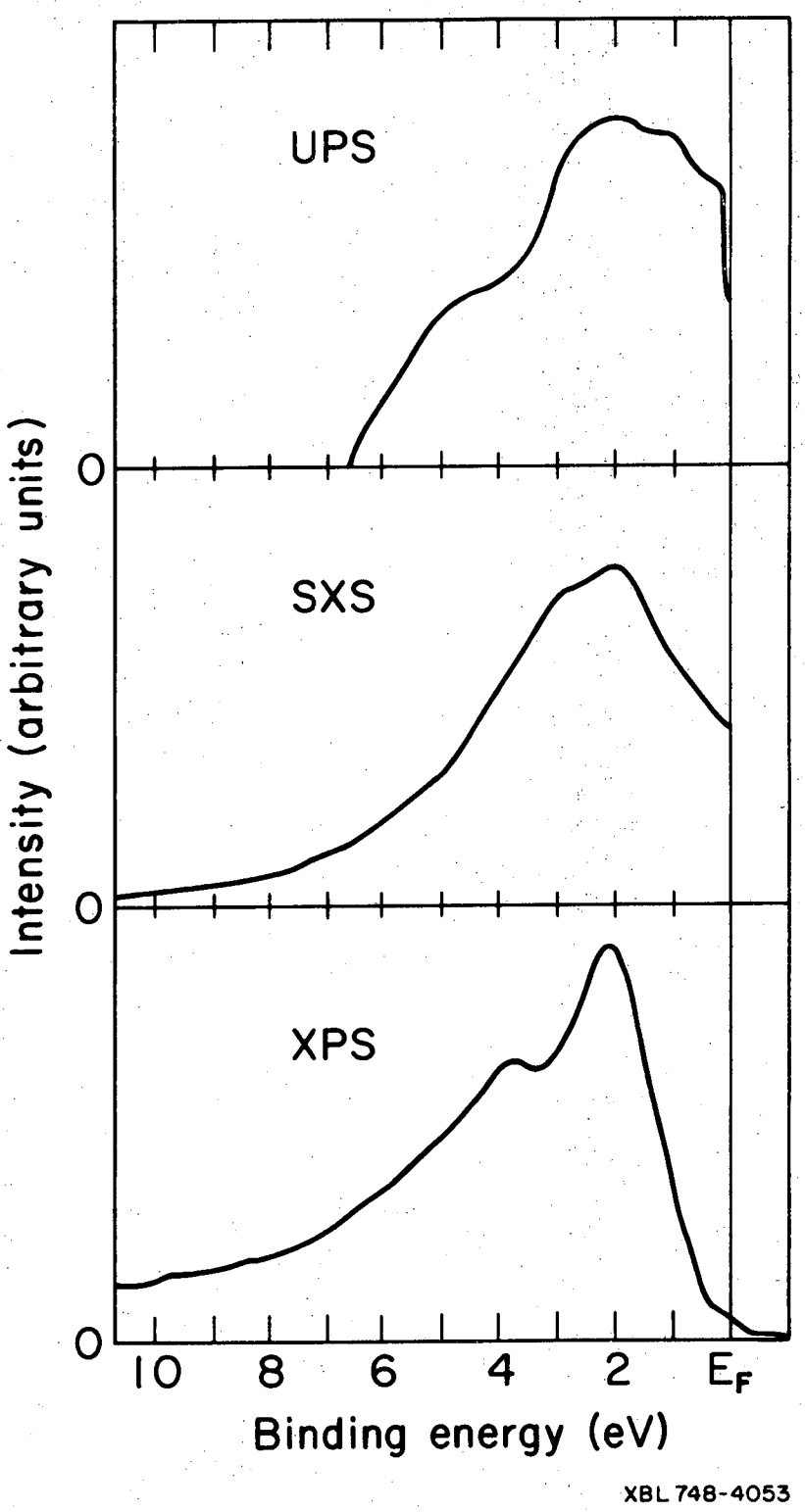
UPS
SXS
XPS
0
0
0
Intensity (arbitrary units)
10
8
6
4
2
E_F
Binding energy (eV)
XBL 748-4053

Fig. 4

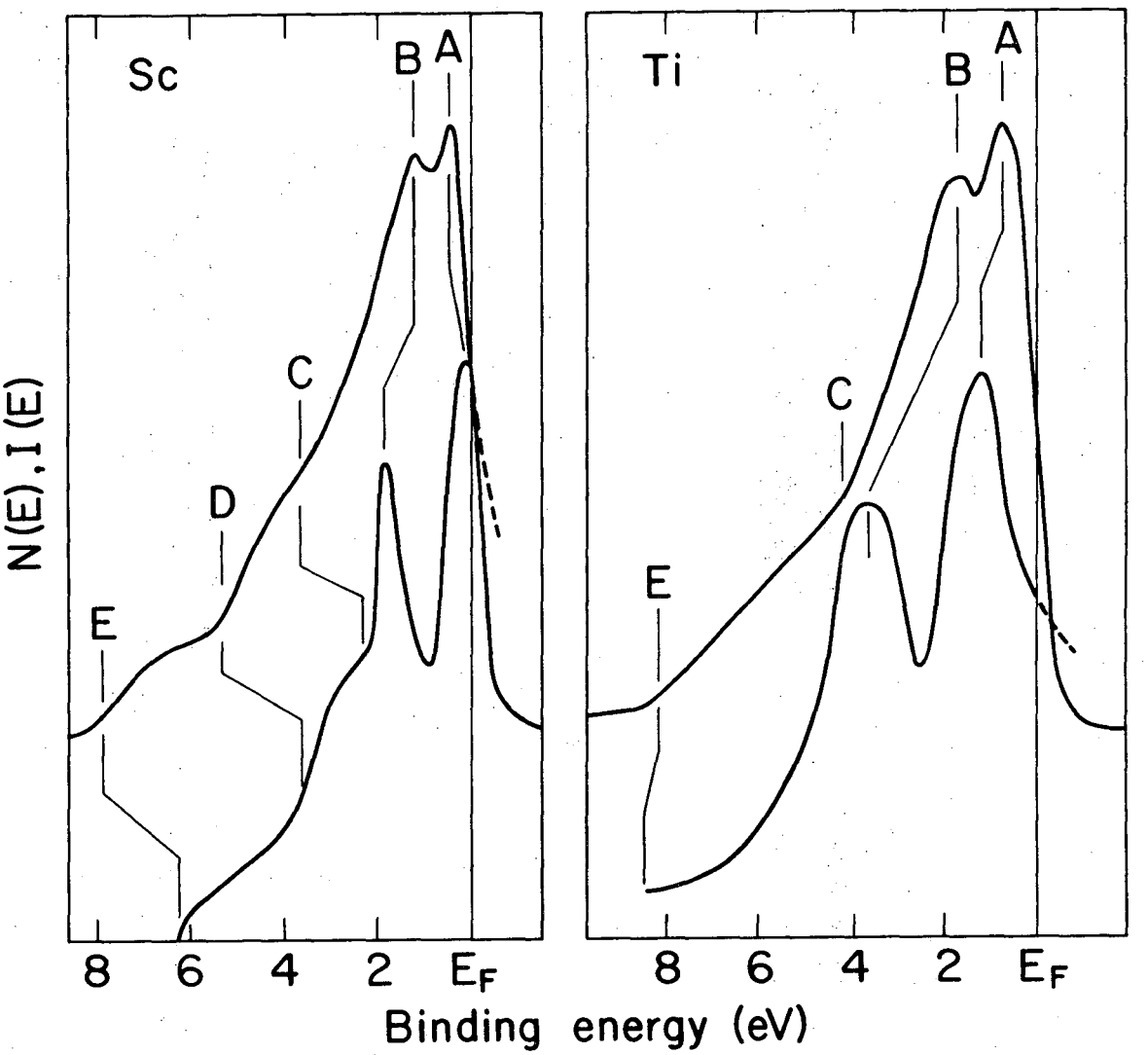
Sc
B
A
C
D
E
N(E), I(E)
8
6
4
2
E_F
Ti
B
A
C
E
8
6
4
2
E_F
Binding energy (eV)
XBL 747-3648

Fig. 5

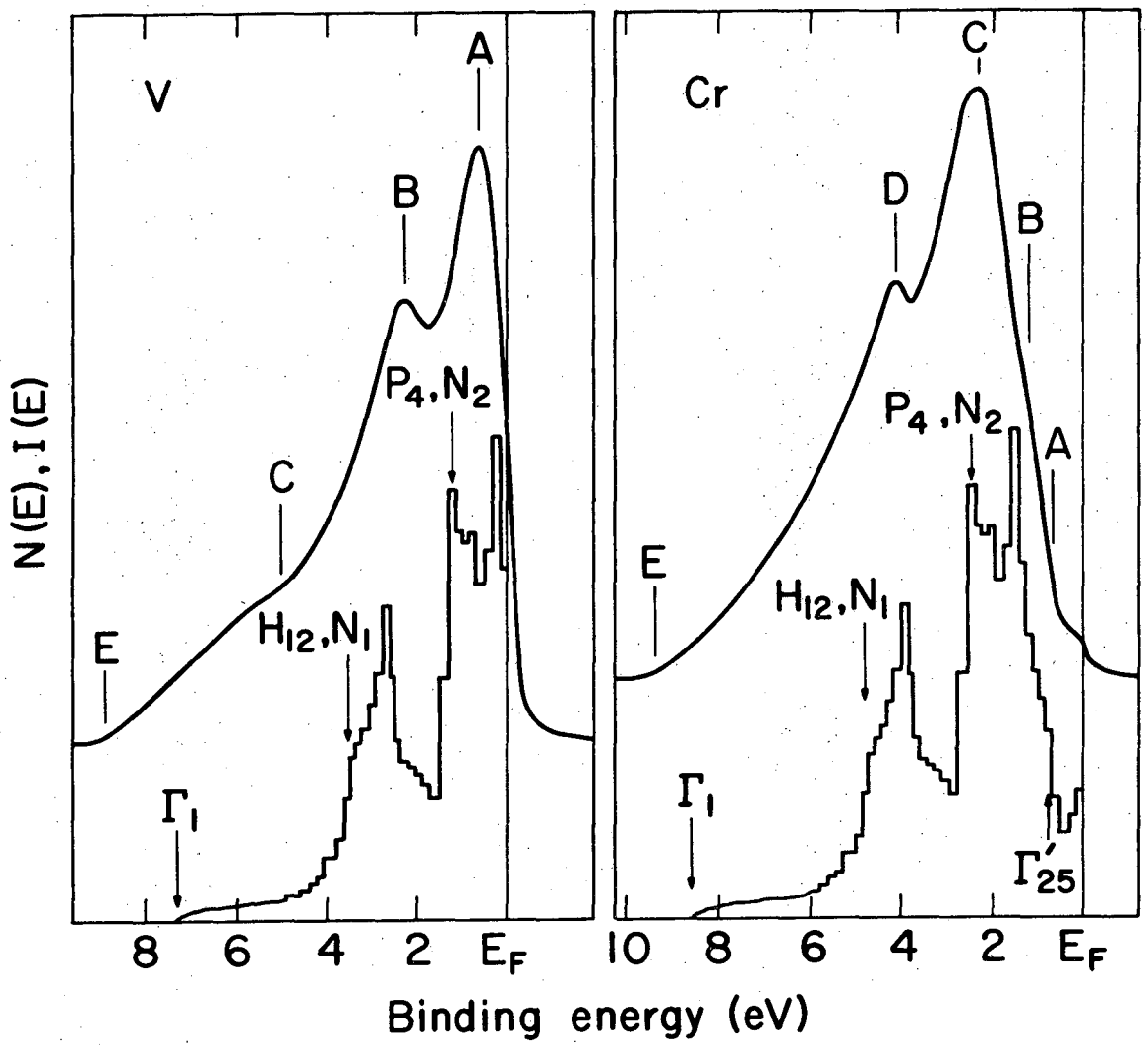
V
A
B
C
P4,N2
H12,N1
E
Γ1
N(E), I(E)
8
6
4
2
EF
Cr
C
D
B
P4,N2
A
E
H12,N1
Γ1
Γ'25
10
8
6
4
2
EF
Binding energy (eV)
XBL 747-3647

Fig. 6

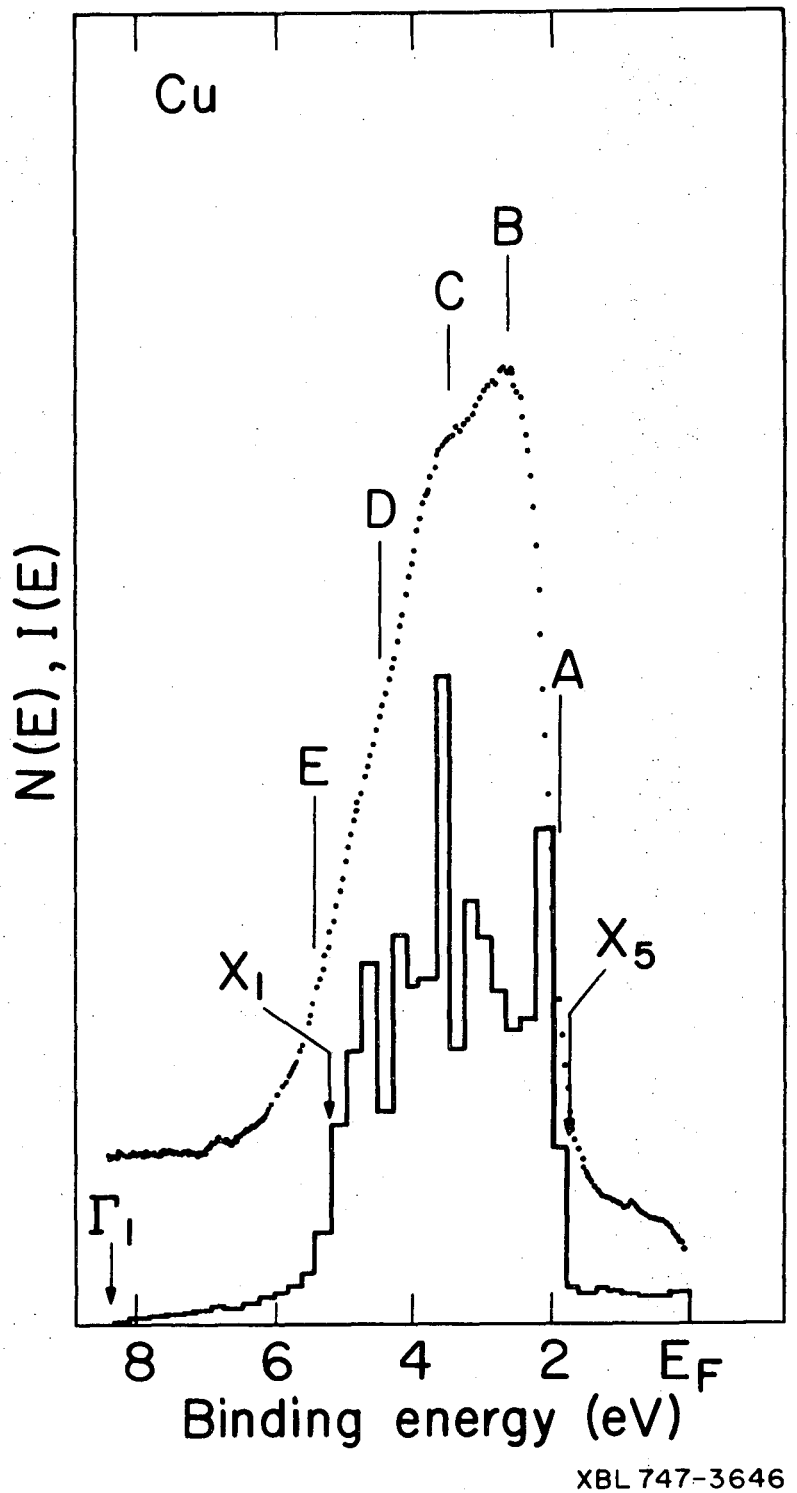

Fig. 7

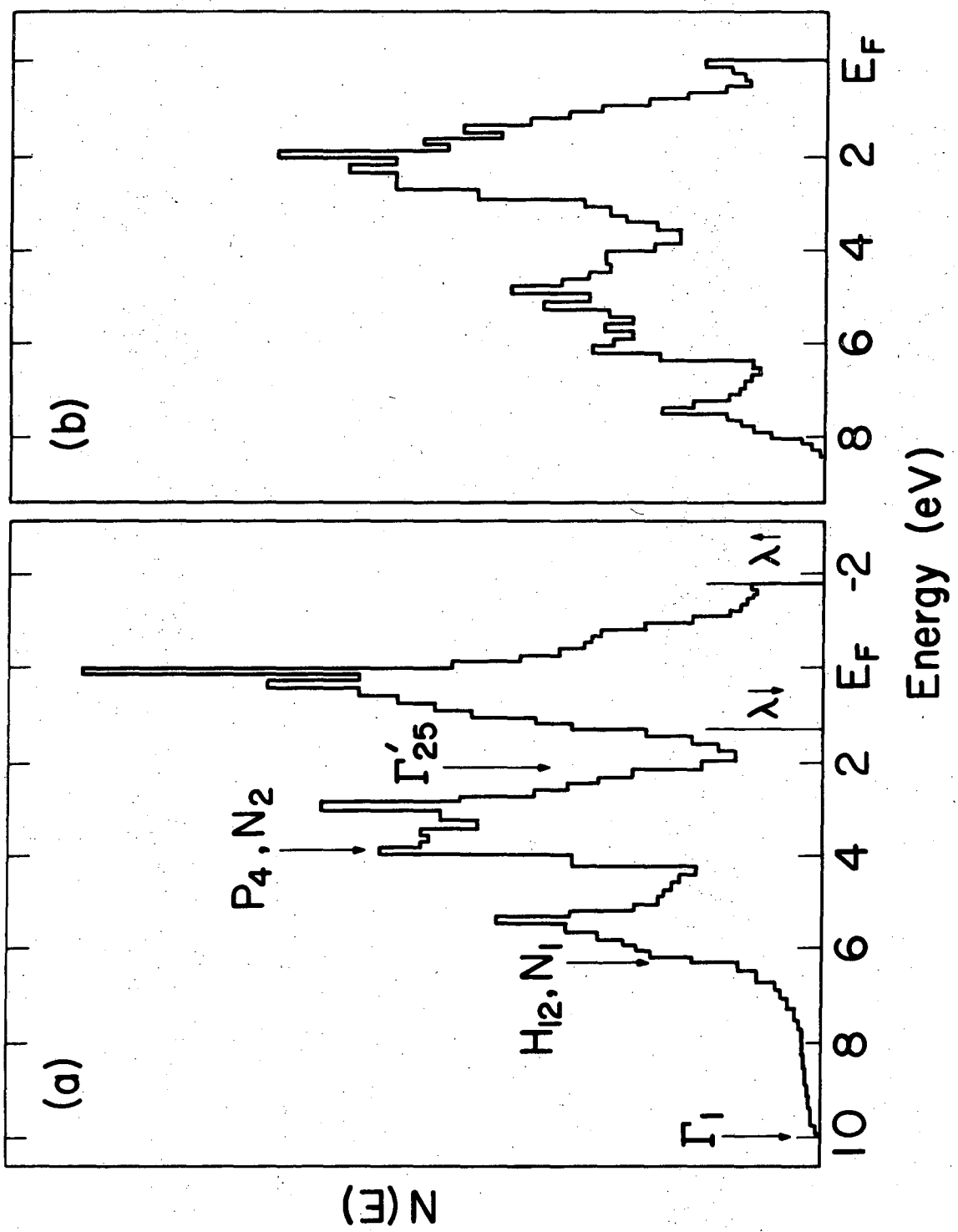
(a)
(b)
N(E)
Energy (eV)
E_F
Γ_1
H_{12}, N_1
P_4, N_2
Γ'_{25}
λ
λ'
10
8
6
4
2
-2
XBL 747-3644

Fig. 8

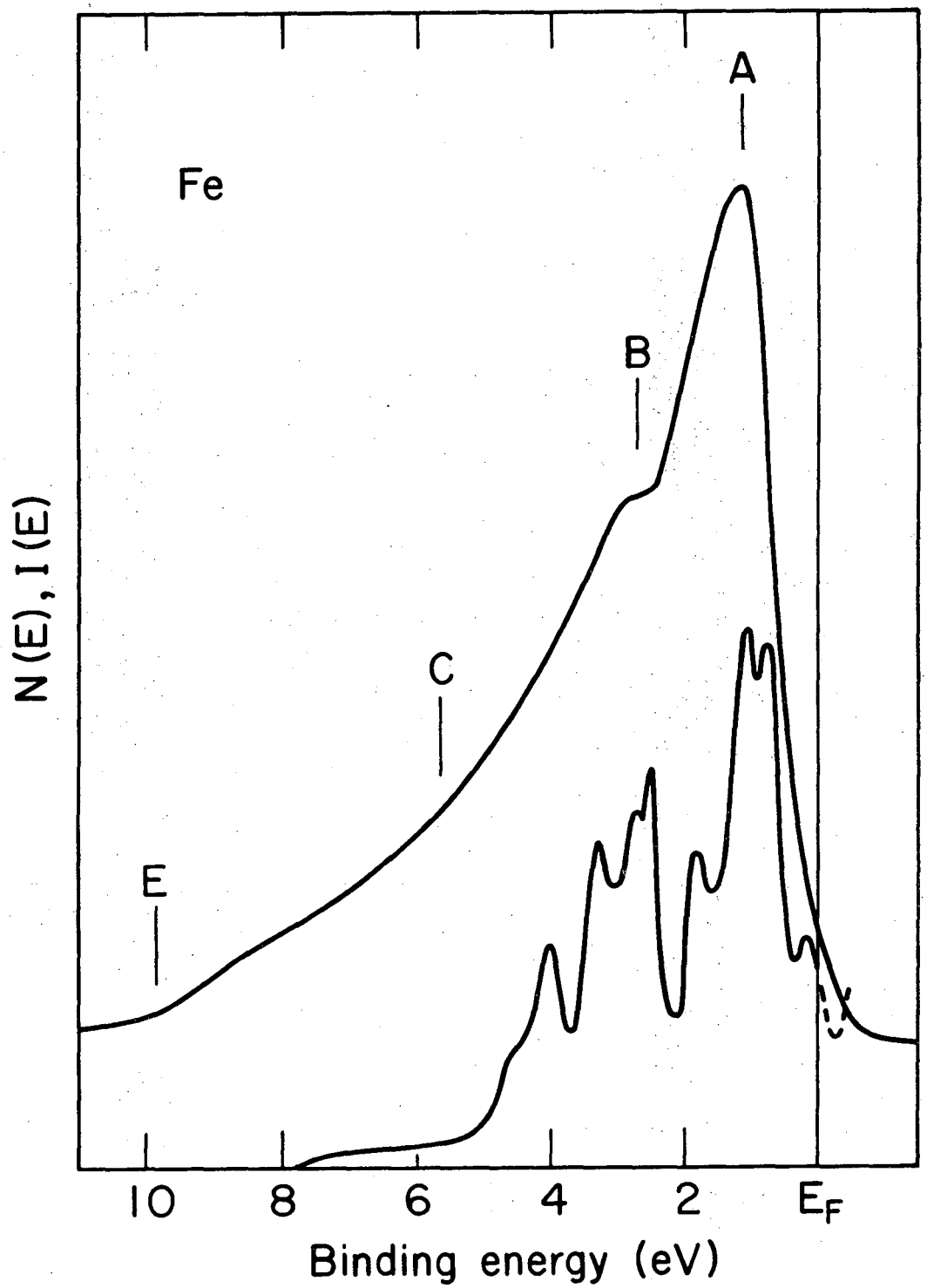

Fig. 9

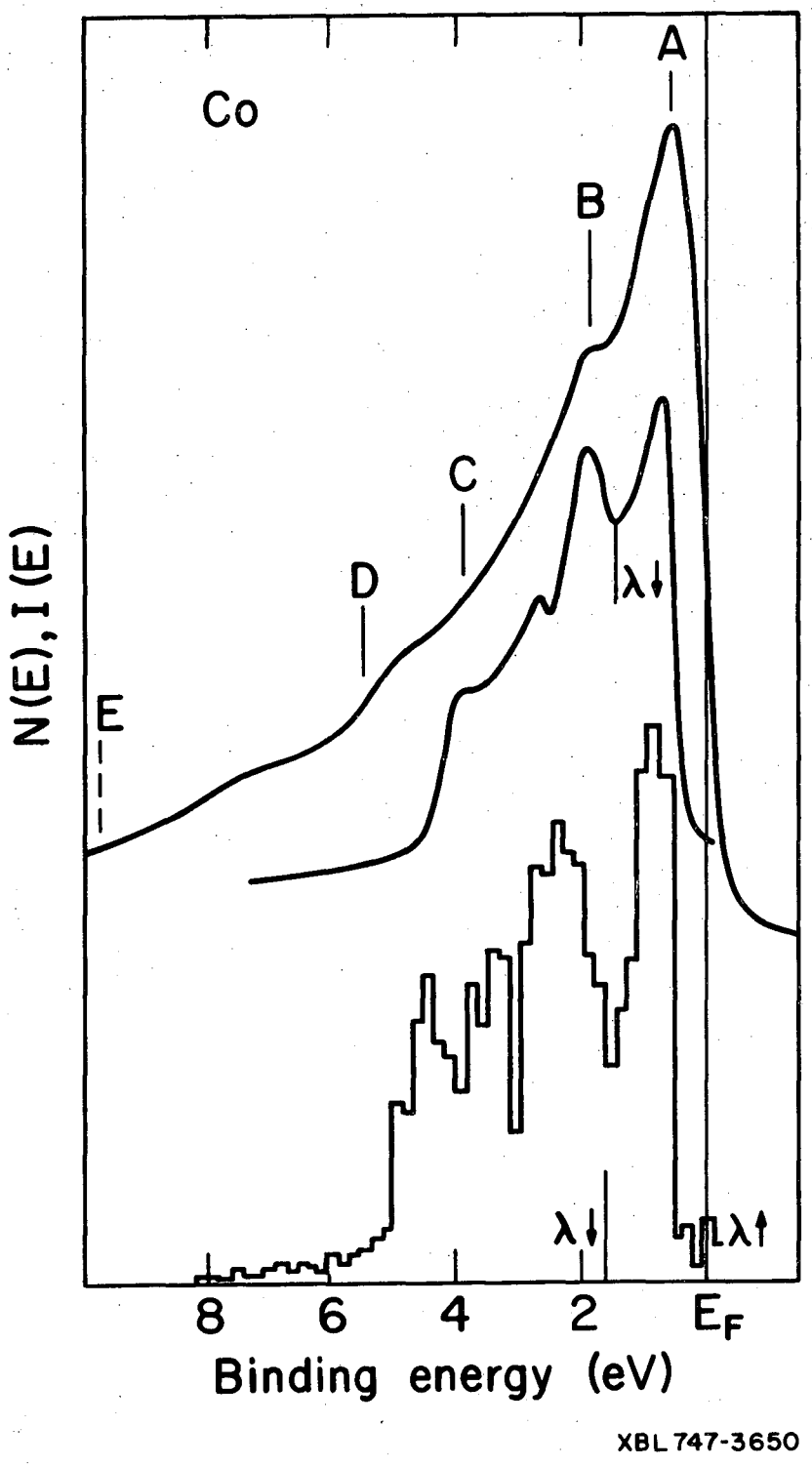

Fig. 10

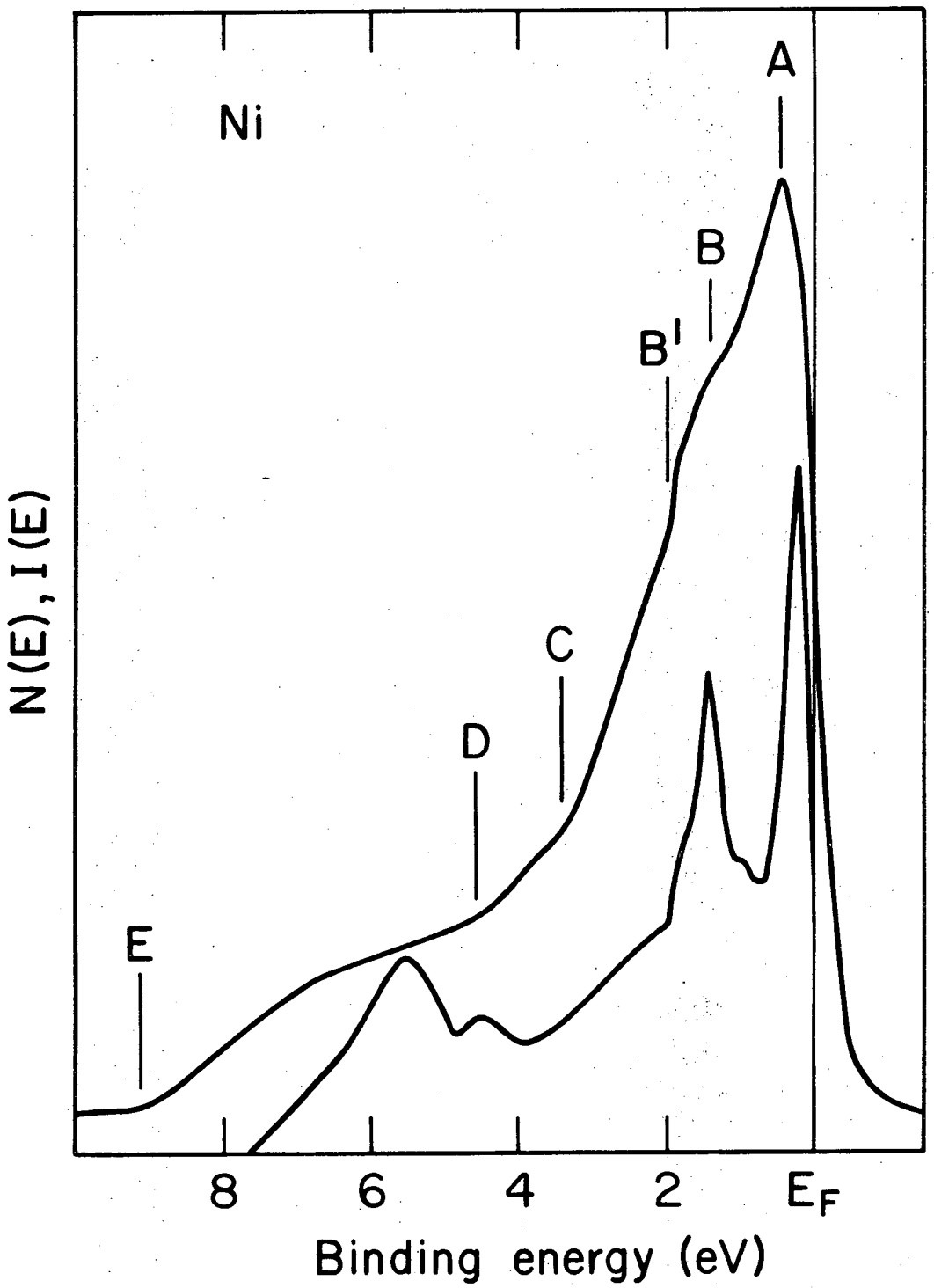

Fig. 11

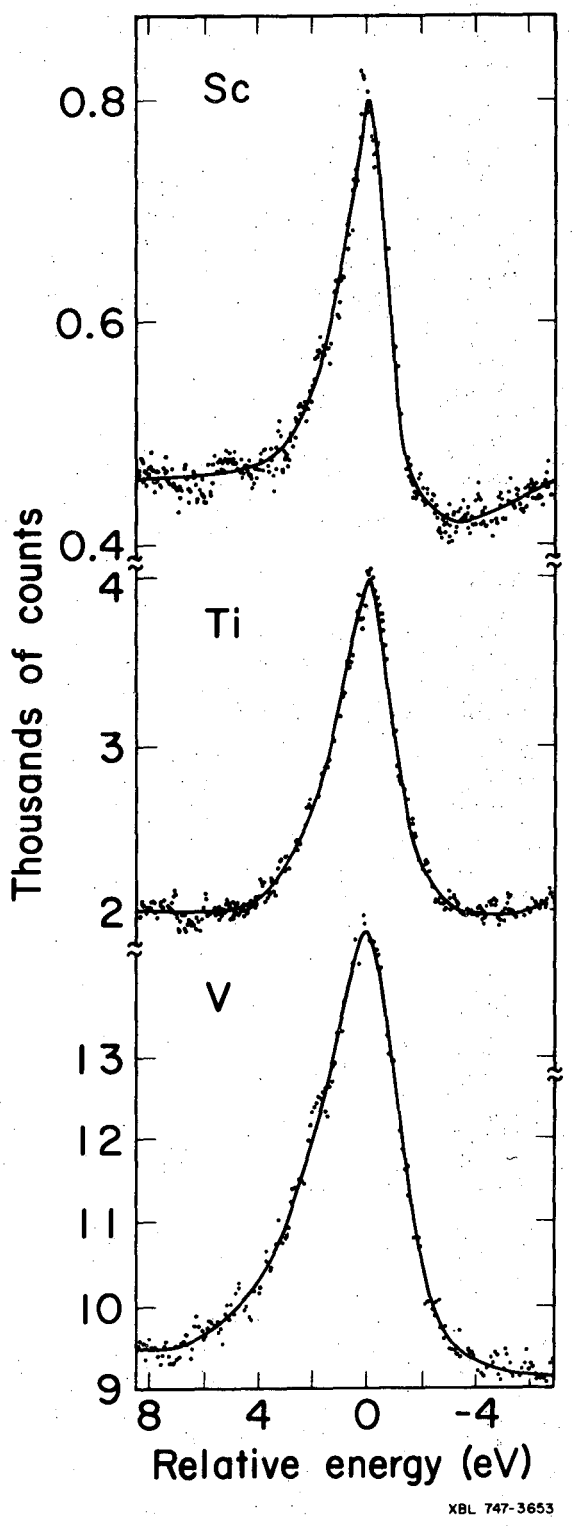
Sc
Ti
V
0.8
0.6
0.4
4
3
2
13
12
11
10
9
Thousands of counts
8
4
0
-4
Relative energy (eV)
XBL 747-3653

Fig. 12

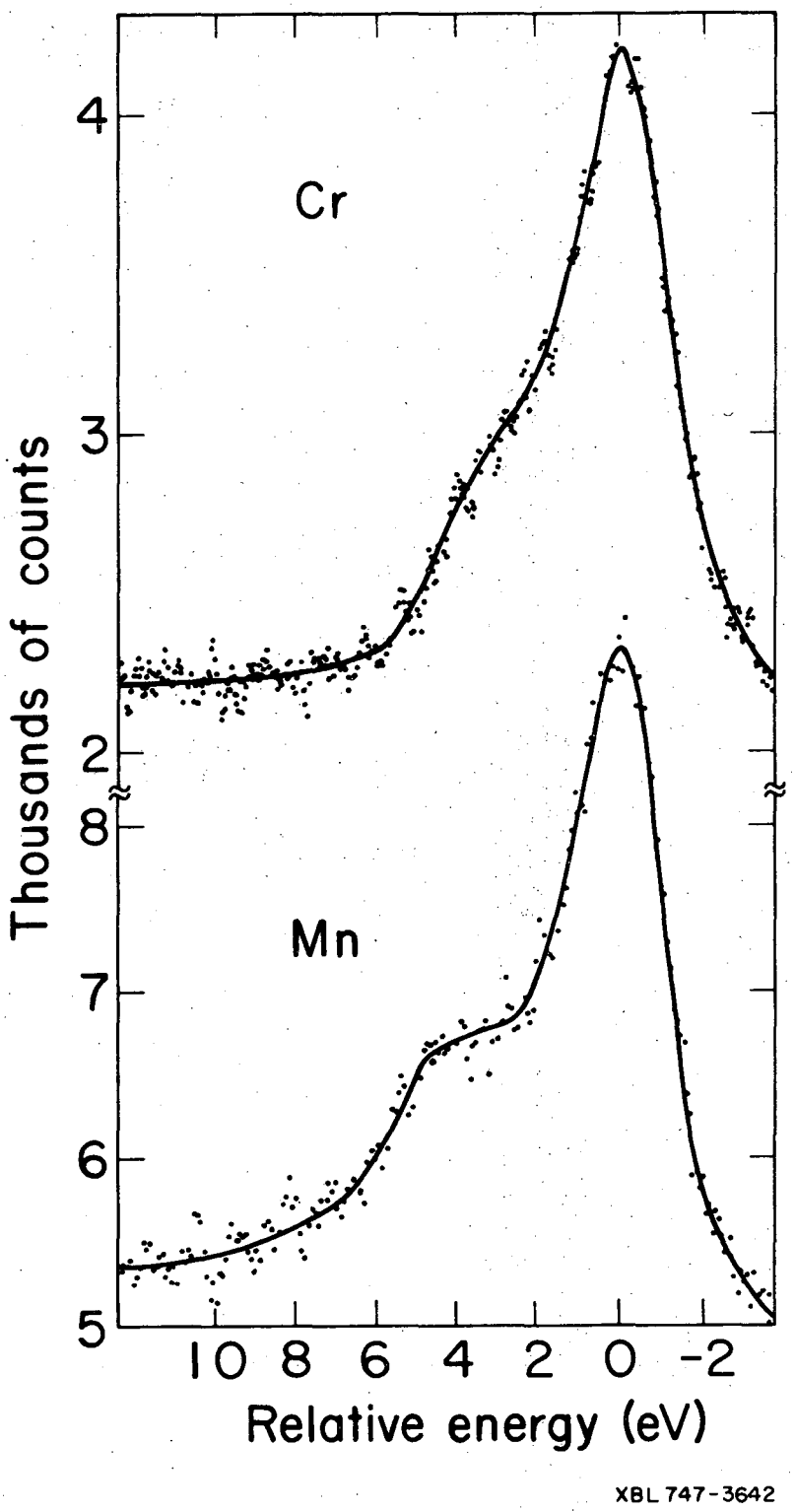
Cr
Mn
Thousands of counts
4
3
2
8
7
6
5
10 8 6 4 2 0 -2
Relative energy (eV)
XBL 747-3642

Fig. 13

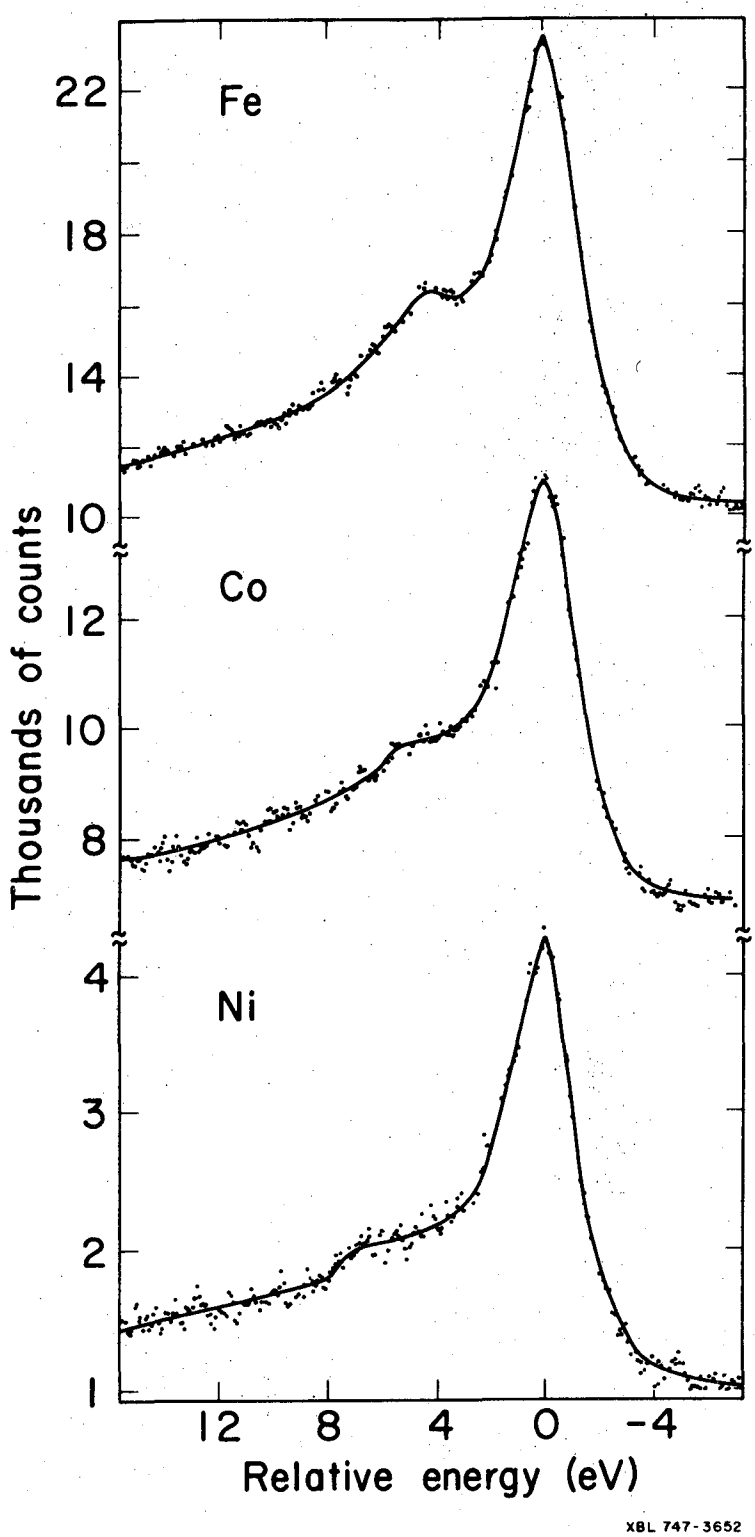
Fe
Co
Ni
Thousands of counts
22
18
14
10
12
10
8
4
3
2
1
12
8
4
0
-4
Relative energy (eV)
XBL 747-3652

Fig. 14

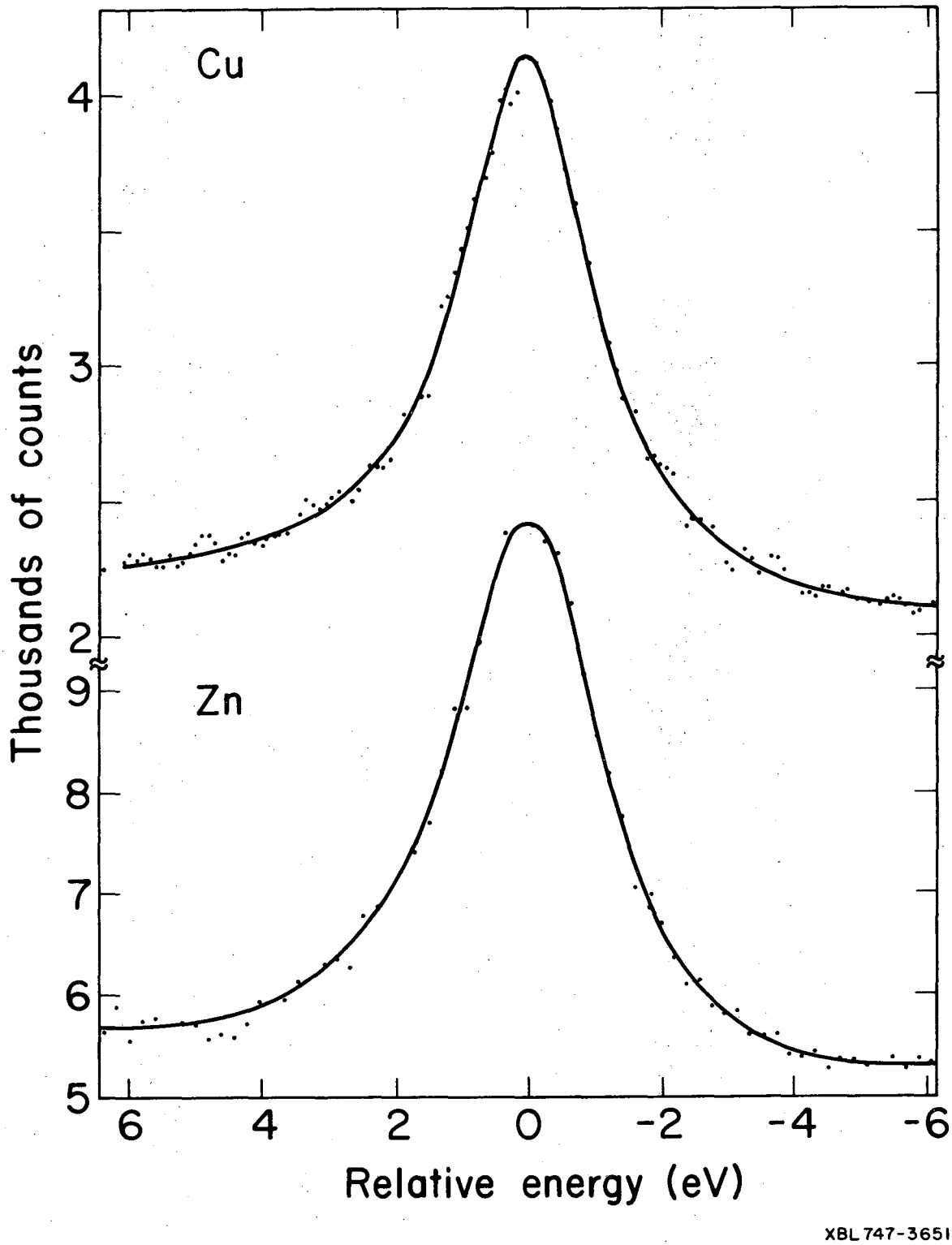
Cu
Zn
Thousands of counts
4
3
2
9
8
7
6
5
6
4
2
0
-2
-4
-6
Relative energy (eV)
XBL747-3651

Fig. 15

TECHNICAL INFORMATION DIVISION
LAWRENCE BERKELEY LABORATORY
UNIVERSITY OF CALIFORNIA
BERKELEY, CALIFORNIA 94720